 Bull. Chem. Soc. Jpn., **76**, 689–708 (2003)

Accounts

Porphyrin Supramolecules for Artificial Photosynthesis and Molecular Photonic/Electronic Materials

Yoshiaki Kobuke* and Kazuya Ogawa

Graduate School of Materials Science, Nara Institute of Science and Technology, CREST (Core Research for Evolutional Science and Technology) of Japan Science and Technology Corporation, 8916-5 Takayama, Ikoma, Nara 630-0101

(Received October 9, 2002)

Porphyrin supramolecules were constructed by ligand coordination to central metal ions, hydrogen bonding, or chelate complexation to external metal ions. *meso-N*-Methyl-2-imidazolyl-substituted porphyrin afforded a special pair model and a light-harvesting antenna mimic by complementary coordination of imidazolyl to Zn and Mg, respectively. Characteristic splits of the Soret band in absorption spectra and large upfield shifts of imidazolyl and pyrrolic β protons in the ^{1}H NMR spectra suggested the close proximity of two porphyrin π–π planes. Such upfield shifts in the ^{1}H NMR spectra were also observed for coordination organization of 2,5-dihydroxyphenyl-substituted porphyrinatoMg. As an example of organization by hydrogen bonding, the supramolecular assembly between imidazolyl substituents afforded stacks of porphyrins with antenna function in solution and gave rise to the formation of stable antenna liposome without any lipid components such as lecitin. Mono- and bis(8-hydroxy-5-quinolyl) substituted porphyrins were coordinated with Ga(Ⅲ) to afford tris(oxinato) chelate and poly(oxinato) chelate, respectively. The fluorescence intensity of each Ga complex was increased significantly compared with that of each starting monomer. At the same time, efficient excitation energy transfer among three porphyrins has been observed to realize the light-harvesting function. Novel bipyridylene-bridged bisporphyrin was synthesized by a nickel(0)-mediated homocoupling reaction of bromopyridyl-porphyrinatoZn. Spatial geometries of two porphyrins were regulated by reversible complexation of the bipyridyl part with $PdCl_2$. Bis(imidazolylporphyrinatoZn), which was directly linked at *meso*-position, afforded a giant linear multi-porphyrin array by successive links of complementary coordination of imidazolyl to zinc having molecular weight of 10^5 at a distribution maximum corresponding to 80 bisporphyrin units and at the molecular length of 110 nm. On the other hand, the polyporphyrin can be dissociated to bisporphyrin unit and scrambled with monomeric imidazolylporphyrinatoZn in the presence of MeOH or pyridine to produce oligomers terminated by the monomeric porphyrin. This reorganization process could apply to the systems generating efficient photocurrents and large third-order optical nonlinearity.

The light harvesting (LH) antenna complex in biological photosynthetic system contains many chromophores, mainly bacteriochlorophylls, which are non-covalently arranged in appropriate positions to absorb solar energy and to facilitate the succeeding rapid energy transfer to the reaction center (RC) with high efficiency.[1–3] In the reaction center,[4–9] there is a special pair of chlorophylls to generate an efficient charge separation state after receiving the excitation energy from the antenna. The chlorophylls both in the antenna complex and in the special pair are fixed by membrane proteins through coordination of histidine-imidazole to their central metal ion. These arrangements successfully drive some important biological functions. The full set-up of the system will be shown schematically as in Fig. 1.[10] These beautiful chromophore assemblies have inspired many chemists to construct artificial photosynthesis systems in order to understand the complex energy/electron transfer mechanisms and to elucidate the basic principles as well. Success in the construction of artificial photosynthesis will also contribute to

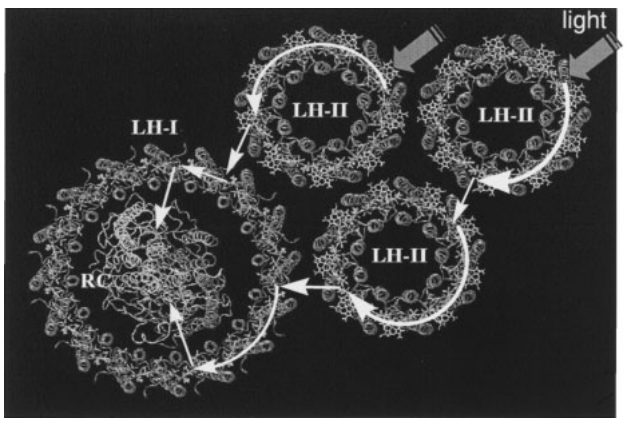

Fig. 1. Schematic drawing of the bacterial light-harvesting complex LH2 and LH1 containing reaction center (RC) from photosynthetic bacteria.[10]

the development of practical applications of the solar cell; then clean solar energy will be available permanently.

Current attention is also focused on molecular electronic and photonic devices.[11–15] Since miniaturization of LSI built by metal-oxide-semiconductors (MOS) is close to its practical limit,[14] molecular-scale devices, which may provide high performance computers,[15] are now absolutely required. One of the possibilities for the material to build up such the device is a nanometer-scale organic single molecule with high conductivities, such as carbon nanotube[16,17] and multi-porphyrin array.[18] The large conjugated π-electron system of porphyrins is interesting not only in view of small HOMO–LUMO energy gap, but of light-absorbing and emitting properties which allow us to obtain desirable electronic and photonic materials.

Third-order nonlinear optical (NLO) materials have also attracted attention because of their potential utilities for photonic applications such as ultrafast optical switching and modulations.[19–21] Various types of organic compounds have so far been designed and synthesized to obtain materials with large third-order susceptibilities $\chi^{(3)}$.[22–24] Porphyrins are one of the most promising candidates for such NLO materials, thanks to the large π-conjugated system, the versatile modifications of the structures, and the various possibilities of central metal ions to design ideal properties.[18,25–33]

Varieties of covalently or noncovalently linked multi-porphyrin molecules have been synthesized to construct artificial photosynthetic mimics[34] and as potential materials for molecular electric wires,[35–41] optoelectronic gates,[42,43] non-linear optics,[29–33] and other purposes.[44–47] Supramolecular approaches to synthesize such porphyrin systems contain noncovalent interactions such as metal-to-ligand coordinate bonds, hydrogen bonds, and electrostatic or hydrophobic interactions. Recent advances in supramolecular chemistry have stimulated us to construct complex molecular systems from simple units. This approach started from our biomimetic interests, because biologically important functions are nicely realized by organizing simple units by weak interactions to demonstrate perfect examples.

We have been trying to synthesize porphyrin systems that simulate the structures and functions of photosynthetic energy and electron transfer systems by using the supramolecular techniques. At first, we have succeeded in constructing a supramolecular porphyrin dimer mimicking the special pair of photosynthetic reaction centers by using complementary coordination of imidazolyl to central zinc.[48] This structural unit has opened the way to further propagated multi porphyrin arrays by changing the central metal ion[49–51] and directly linking two coordination units.[41] The most characteristic feature of this assembly is that the self-assembled porphyrin array can be dissociated into monomeric species or into arrays of appropriate length by adding controlled amounts of a coordinating compound such as MeOH or pyridine. This unique property allowed us to construct desirable porphyrin assemblies exhibiting light harvesting[52] or optical functions[33] by a reorganization process in the presence of specific molecular terminators.

The use of chelate complexation by *meso*-substituted ligands with an external metal ion is also a powerful tool to assemble porphyrins.[53–55] Orientations and environments of porphyrins in the resulting assembly should depend on the geometrical structure around the metal ion, and therefore can be optimized by the choice of some metal ion to show each novel function. Two examples of self-assembled porphyrins by using chelate complex formation and their properties will be introduced in this account.

Another approach is the use of hydrogen bonding. This interaction is relatively weak, but stable aggregations can be formed through cooperative hydrogen bonds at multiple sites, combined with hydrophobic interaction and π–π interaction between porphyin rings. Porphyrin aggregations by use of hydrogen bonding were observed in non-polar solvents[56] and as liposome[57] by well-designed porphyrins of our strategies. In this article, we will present our recent trials of supramolecular porphyrin assemblies aiming at artificial photosynthesis as well as at molecular photonic and electronic devices.

1. Self-Assembly by Complementary Coordination to Central Metal Ion

1.1 Formation of a Slipped Cofacial Dimer. Two chlorophylls of a special pair in the photosynthetic reaction center are fixed in a slipped cofacial orientation with interplanar distances of 3.1–5.0 Å by coordination of histidine imidazolyl to the central metal.[4–9] Light energy absorbed by the antenna complex is transferred finally to the special pair dimer; then highly efficient charge separation initiates the oxidation-reduction sequence in the photosynthetic reaction center. In order to understand the role of dimeric structure in the redox function, several face-to-face porphyrin dimers have been synthesized by covalent[58–61] and non-covalent[48,62–66] connections.

In 1994, we introduced two *N*-methylimidazolyl groups at *meso*-positions of tetraethyltetramethylporphyrin **1** and found that its zinc complex **2** existed quantitatively as a slipped cofacial dimer **3** by the complementary coordination of the imidazolyl to Zn(II) in a nonpolar media such as chloroform (Scheme 1).[48] Since zinc ion accepts only one axial coordination in porphyrin chemistry, further organization can not proceed.

The ^{1}H NMR spectrum of free base **1** was simple and normal for all respects and showed a structure of C_2 symmetry. However, the spectrum of dimer **3** in $CDCl_3$ as shown in Fig. 2 with the chemical shift data of all peaks assigned on the basis of COSY and PROESY measurements showed a dramatic change due to the

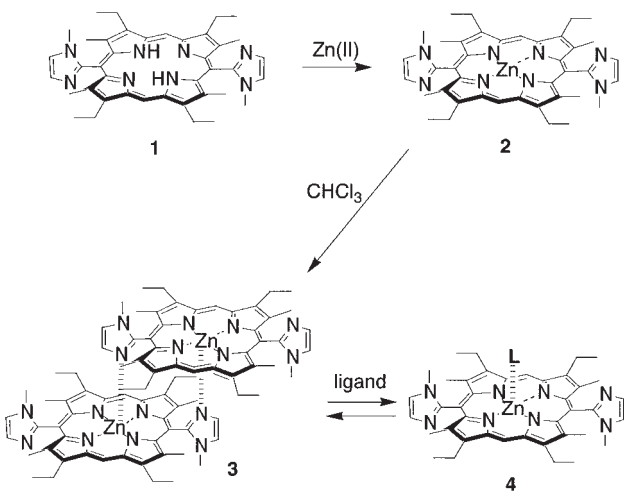

Scheme 1. Formation of self-organized dimer by complementary coordination of imidazolyl to zinc.

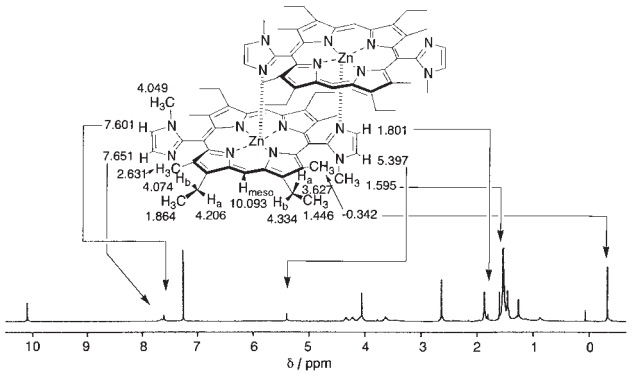

Fig. 2. ^{1}H NMR spectrum of dimer **3** in $CDCl_3$ with the chemical shifts.

exceptionally strong interaction between two stacked porphyrins. All of the protons other than the *meso* protons appeared as a pair with equal intensities; one set of this pair shifted to upper field due to the strong ring current effect of the facing porphyrin. For example, protons of the stacked and nonstacked 4-positions of facing imidazolyl groups appeared at 1.80 and 7.65 ppm, respectively, indicating a remarkable shielding effect ($\Delta\delta =$ 5.85 ppm).

A clear proof of the slipped cofacial arrangement was also exhibited in the absorption spectrum of **3** in chloroform, as shown in Fig. 3. The Soret band was split by 18 nm, suggesting the exiton interaction between two chromophores. The head-to-tail and face-to-face orientations of the transition dipoles $\mu_\perp$ and $\mu_\parallel$ in the slipped cofacial arrangement generate red- and blue-shifts of the Soret band, respectively. The splitting energy ΔE that is correlated with the distance and the orientation of chromophores corresponds to 1035 cm^{-1}, the largest class of splitting in this type of dimer.[58–66] The complementary coordination of imidazolyl to zinc to form the dimer occurred at a highly dilute concentration even at the detection limit of the absorption (10^{-7} M) or fluorescence (10^{-9} M) spectrum. This result indicates that the association constant is at least as high as 10^{10}. On the other hand, even such a very stable dimer in non-polar solvent can be dissociated by adding a competing ligand such as MeOH, imidazole, or pyridine to monomeric species **4** (Scheme 1). This simple process to control complexation equilibrium enables us to perform the structural change for applications such as molecular wire (see section 4.1–4.3).

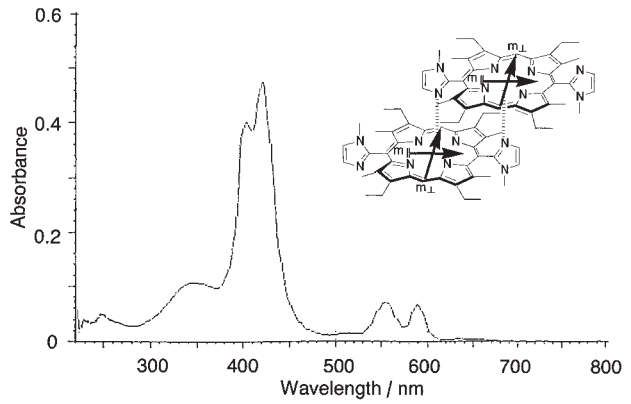

Fig. 3. Absorption spectrum of **3** in $CHCl_3$.

Recently, we determined the three-dimensional structure of complementary coordination by using dimer **5** with different substituents at β- and *meso*-positions, as shown in Scheme 2, by X-ray crystallography.[67] As expected from NMR and spectral data, two porphyrins are stacked in the slipped cofacial arrangement, with a metal-metal distance of 6.13 Å and an interplanar distance of 3.23 Å. Table 1 compares the structural parameters of **5** with those of special pairs in biological system.[4–9] The distances between two metal centers and the interplanar distance of dimer **5** are similar to those of natural special pairs. Especially the interplanar distance of **5** belongs to the smallest class, suggesting a good mimic of a natural special pair with strong interaction of two chromophores. Interestingly, the one-electron oxidation potential of **3** was 63 mV lower than that of monomeric Zn(OEP) in CH_2Cl_2 (OEP = octaethylporphyrin). The lower oxidation potential of this dimer may come from the strong interaction of two porphyrins. Since the special pair in nature works as a one electron donor to form the charge separated state, lower oxidation potential is considered to be advantageous to generate the charge separated species more efficiently than a monomer can. The role of special pair for attaining efficiently the long-lived charge-

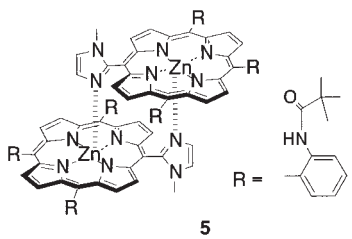

5

Scheme 2. Molecular structure of **5**.

Table 1. Comparison of Metal–Metal Distance and Interplanar Distance with Those of Special Pair in Nature

Entry	Interplanar distance/Å	Distance between metal centers/Å	Reference
5	3.23	6.13	This work[67]
P700 (PS I of thermophilic cyanobacterium *S. elongatus*)	3.6	6.3	9
P680 (PS II of thermophilic cyanobacterium *S. elongatus*)	5.0	10.0	8
P875 (*Rhodobacter sphaeroides* R26)	3.5	7.5	5
P960 (*Rhodopseudomonas viridis*)	3.1	7.4	7

separated state is now under investigation by using the complementary dimer model and results will be reported elsewhere.

1.2 Construction of Self-Assembled Porphyrin Oligomer by Using Mg(II). X-ray crystallographic study of the light-harvesting antenna complex B850 from photosynthetic bacteria revealed a beautiful ring structure having a supramolecular arrangement of eighteen bacteriochlorophylls to gain light energy and transfer the excited energy to the reaction center efficiently.[1] Figure 4 shows a simplified drawing of this supramolecular arrangement. Each chlorophyll molecule is partially overlapped with neighboring chlorophylls in a slipped arrangement by the coordination of imidazolyl from histidine residue again. In the above section, we demonstrated the self-organization by complementary coordination of imidazolyl to zinc, which prevented further organization. Here, we tried to introduce Mg instead of Zn as the central metal ion,[49] since Mg(II) could accept the hexacoordination and extend the structural organization further, as shown in Scheme 3.

NMR study of the self-organized complex of Mg porphyrin **6** in $CDCl_3$ showed a growth of the coordination structure by the continuous repetition of hexacoordination. However, the mean assembly number was determined as 2.4, which corresponds roughly to the existence of 60% dimer and 40% trimer. Extension of the porphyrin aggregate seems to be limited by the relatively low solubility of the assembled species.

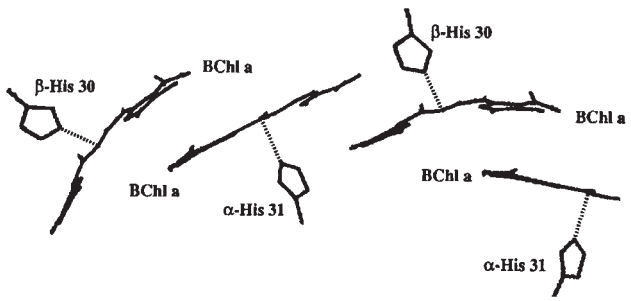

Fig. 4. Structural organization of bacteriochlorophylls in antenna complex B850 from photosynthetic bacteria. The original picture in Ref. 1 was modified to illustrate the organization schematically.

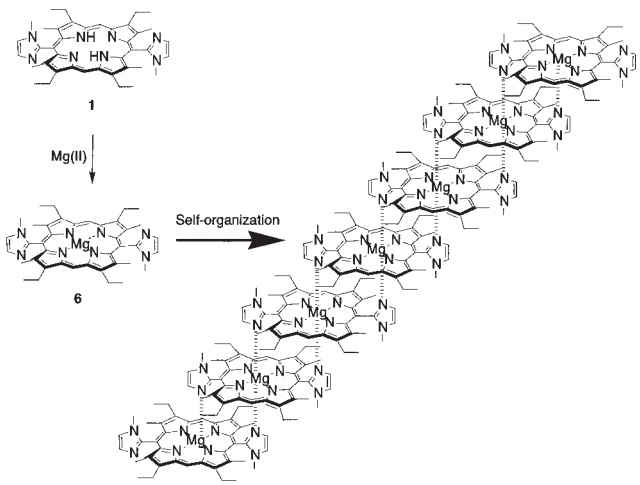

Scheme 3. Formation of self-organized oligomer by complementary coordination of imidazolyl to Mg.

In order to detect the elongation of organized structure, we have measured the FT ion spray mass spectrum.[51] When the spectrum was obtained from a MeOH solution, the trimer species were observed as the largest mass number, along with peaks of monomer, dimer and dicationic trimer/2. Then the sample solution was changed to MeOH/$CHCl_3$ (1/1) to favor the observation of larger aggregates. A series of peaks up to pentamer was observed. Tetramer and pentamer peaks were detected only at the corresponding half molecular weights with increments of 0.5 mass units, indicating the ionization as dicationic species. Figure 5 shows the positive ion mode ESI mass spectrum in the region corresponding to dimer, trimer, tetramer, and pentamer (MW 1321, 1982, 3304, and 4625, respectively) from MeOH/$CHCl_3$ (1/1) solution. In Fig. 5B, dimer peaks with increments of one mass unit were overlapped with dicationic tetramer peaks with increments of 0.5 mass unit. When the spray voltage was lowered to facilitate the observation of higher aggregates, dicationic heptamer peaks could be detected, as shown in Fig. 5D. These results demonstrated that Mg(II) metal center can accept the 6-th coordination from imidazole ligand and thus can be extended to large oligomers.

1.3 Self-Organization by Hydroquinone. Bis(imidazolyl)porphyrin Mg complex gave a growth of the slipped cofacial coordination structure to some extent. Since Mg accepts oxygen ligand as well as imidazolyl nitrogen, as seen in chlorosomes, the light-harvesting system of green bacteria, hydroquinone was introduced as a *meso*-substituent and examined in the search for another type of molecular organization of Mg porphyrins, as shown in Scheme 4.[68]

Absorption and fluorescence spectra of free base **7** and Mg complex **8** did not show any remarkable splitting or shift of peaks compared with H_2TPP and MgTPP, respectively, indicating that **8** exists as a monomeric form in a dilute concentration range such as was employed for absorption and fluorescence measurements. However, NMR studies revealed complexation behavior at a higher concentration range of 2.5×10^{-4} to 8×10^{-3} M. Figure 6 shows ^{1}H NMR spectra of free base **7** (A) and Mg complex **8** (B). β-Pyrrole protons that appeared at 8.90 ppm (8H) for **7** split into two doublets at 8.68 and 8.47 ppm (2H each) and

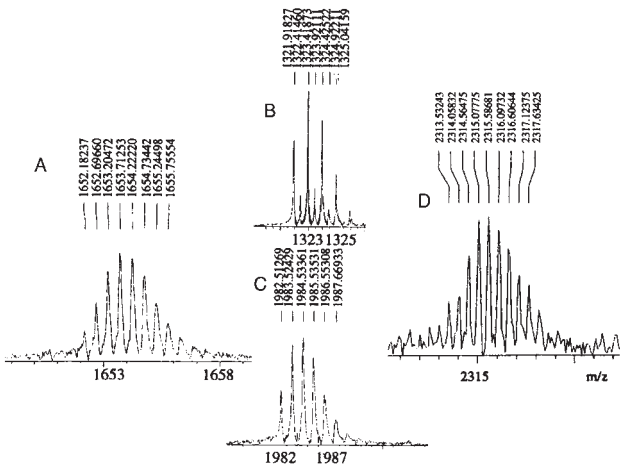

Fig. 5. ESI Mass spectra in the areas corresponding to A) pentamer (dication), B) tetramer (dication) with dimer (monocation), C) trimer (monocation), and D) heptamer (dication).

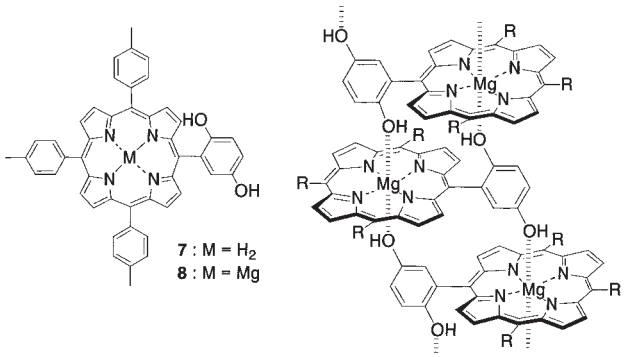

Scheme 4. A proposed structure of mono(2,5-dihydroxyphenyl)-porphyrin Mg complex (R = *p*-tolyl).

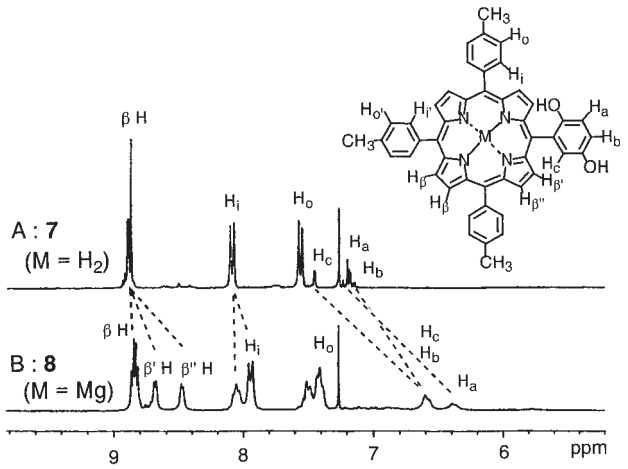

Fig. 6. ^{1}H NMR spectra of free base **7** (A) and Mg complex **8** (B) in $CDCl_3$ (8 mM, 20 °C).

multiplets at 8.84 ppm (4H) for **8**. Tolyl protons that appeared as A_2B_2 at 8.06 (6H, H_i and H_i') and 7.56 (6H, H_o and H_o') ppm for **7** also split into two groups, in which two sets of multiplets were observed at 8.03, 7.93 ppm and 7.49, 7.41 ppm. The protons assigned to the hydroquinone part: H_a, H_b, and H_c, shifted more characteristically from 7.21, 7.16, and 7.45 ppm to 6.58 (2H) and 6.38 (1H) ppm, respectively. Since the large shift of the hydroquinone part makes it difficult to correlate each proton directly from the spectrum, the shift-correlation was obtained from the concentration dependence of these peaks. Temperature dependent NMR study down to −40 °C elucidated considerable upfield shifts for all protons in the order:

$$H_a \approx H_c > H_b \approx H_{\beta'} > H_{\beta''} \approx H_i \approx H_o > H_{i'} > H_{o'} > H_\beta$$

The largest shifts on lowering the temperature were observed for 2,5-dihydroxyphenyl peaks H_c and H_a, showing a tendency similar to that of the concentration change. These observations suggest that the molecular organization of Mg porphyrin follows a slipped cofacial arrangement.

2. Self-Assembly by Hydrogen Bonding

2.1 Stack of Bis(imidazolyl)porphyrin by Imidazole–Imidazole Hydrogen Bonding in Solution. In this section, we present bis(imidazolyl)porphyrin **9** as a mimic of light harvesting antenna function by supramolecular assembly formation through hydrogen bonds between 4(5)-imidazolyl substituents at two facing *meso*-positions of the porphyrin ring.[56] 5,15-Bis(imidazolyl)porphyrin **9** was prepared from α-[4(5)-imidazolyl]-2,2′-dipyrrylmethane and 4-dodecyloxybenzaldehyde as shown in Scheme 5.

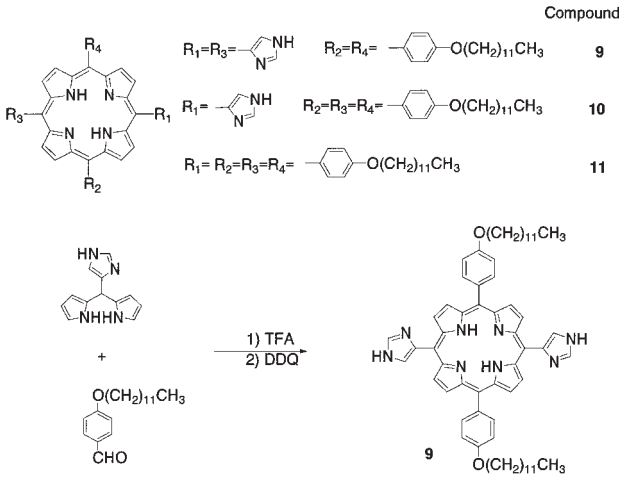

Scheme 5. Structure and preparation of bis(4-imidazolyl)porphyrins.

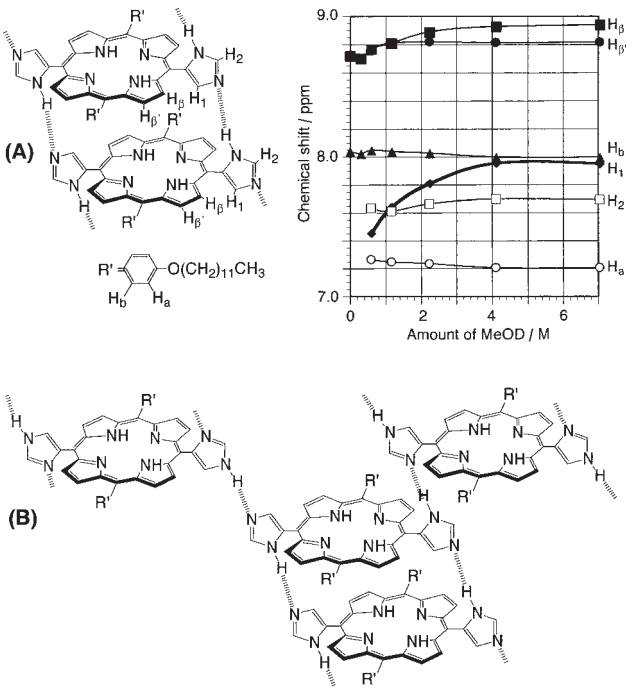

Fig. 7. (A) Schematic drawing of slipped cofacial arrangement self-assembled by hydrogen bonds and NMR titration of **9** (4 mM) in $CDCl_3$ with CD_3OD at 20 °C. (B) Another possible elongation by imidazolyl-imidazolyl hydrogen bonds.

^{1}H NMR spectrum of **9** in $CDCl_3$ gave broad peaks, which were sharpened gradually by the addition of CD_3OD. Figure 7 shows the titration behavior of imidazolyl, pyrrolic, and aromatic protons. The characteristic up-field shift with decreasing CD_3OD concentration was observed most significantly at the imidazolyl proton (H_l), and less at one of the β-pyrrole protons (H_β). The shift behavior is accounted for by gradual breakage of hydrogen

bonds between imidazolyl substituents on the addition of CD_3OD. The selective shielding of the H_1 proton compared to the H_2 in the assembly suggests that H_1 is brought into the facing porphyrin plane by hydrogen bond formation between imidazolyl substituents of different porphyrins (Type A in Fig. 7). Therefore, the slipped cofacial arrangement **9** is proposed as the structural unit of hydrogen-bonded porphyrin rather than the head-to-tail one. The former orientation can be stabilized by the cooperative nature of hydrogen bonds of imidazoles of adjacent porphyrins and π-stacking of porphyrins and is thought to be more stable. In accord with this orientation, H_β proton received the second largest upfield shift with decreasing CD_3OD concentration. At the same time, type B interaction may not completely be excluded from possible existing species, considering the small energy differences between two species. In contrast to these, monoimidazolyl-substituted porphyrin **10**, gave a quite normal NMR spectrum without any specific shielding or peak broadening.

This porphyrin-porphyrin interaction reflected sensitively in their UV spectra. Characteristics of the Soret band of **9** are compared with those of mono- and non-imidazolyl-substituted porphyrins **10** and **11**, respectively, in Table 2. Significant broadening of the half bandwidth (hbw) of **9** (29 nm) in a $CHCl_3$ solution (free from EtOH) was compared with that of **10** (16 nm) in the same solvent. A further broadening was observed in toluene for **9**, but similar solvent dependence was no longer detected for **10**. This behavior is explained by the exciton coupling theory for two porphyrin chromophores in a slipped cofacial orientation,[48,69] where two transition moments interact in face-to-face and parallel orientations to give rise to blue and red shifts, respectively, as discussed in Section 1.1. In the case of **11**, because it has no hydrogen-bonding group, no solvent dependence was observed for the variation of MeOH, $CHCl_3$, and toluene either for absorption maxima or for half bandwidths. Monoimidazolyl-substituted porphyrin **10** seems to be too weak to interact significantly in this fashion and showed the behavior similar to that of the unsubstituted porphyrin **11** in the range 2×10^{-3}–4 mM. This may suggest the cooperation of hydrogen bonds and π-stacking interactions in this supramolecular structure formation.

Interestingly, the fluorescence intensity of bis(imidazolyl)porphyrin **9** remained almost constant for the change of solvent from MeOH to toluene, as shown in Table 3. This result indicates that bis(imidazolyl)porphyrin **9** in the supramolecular assembly showed no significant self-quenching by supramolecular complex formation.

Then, the efficiency of energy/electron transfer from the assembly to external acceptors was estimated by fluorescence quenching experiments. Stern–Volmer plots for two acceptor molecules, chloranil and tetraphenylporphyrinatoMn(Ⅲ) chloride (ClMnTPP) in toluene, were illustrated in Figs. 8a and b, respectively, together with a plot obtained by using non-imidazolyl substituted porphyrin **11** as the reference. Chloranil quenched the fluorescence of **9** 2.9 times faster than it quenched that of **11**. This result suggests that the supramolecule **9** is a more efficient energy/electron donor than the monomeric species. There is a possibility, however, that chloranil becomes a better acceptor through the formation of an intimate hydrogen-bonded complex by using the imidazolyl part of **9**, but not in the case of **11**. However, this possibility was safely excluded by using ClMnPP, which has no hydrogen bond sites but still quenched the fluorescence of **9** more efficiently than that of **11** by exactly the same factor of 2.9. Efficient energy and/or electron transfer from the supramolecule may be explained by the idea that the excitation energy can be delocalized over the whole space of the supramolecule and can be transferred to acceptors from any components of the supramolecule, as in the (8-hydroxy-5-quinolyll)porphyrin[53] below. These results establish the usefulness of supramolecular porphyrin assembly as a mimic of the energy storage function of light-harvesting antenna complexes.

Table 2. Comparison of Absorption Spectral Characteristics of **9** and Porphyrin Analogues in Various Solvents

	λ_{max} (Half bandwidth)/nm			
Compound	MeOH	$CHCl_3$#	Toluene	Cyclohexane
9	418 (24)	424 (29)	426 (34)	426 (84)
10	419 (16)	424 (16)	424 (16)	422 (18)
11	421 (13)	420 (13)	420 (13)	420 (13)

[porphyrin] = 1.6 μM; # EtOH free $CHCl_3$ was used.

Table 3. Comparison of Fluorescence Intensities of **9** in Various Solvents

	Relative intensity (λ_{max}/nm)			
Compound	MeOH	$CHCl_3$#	Toluene	Cyclohexane
9	507 (662)	442 (668)	428 (669)	36 (664)

EtOH free $CHCl_3$ was used.

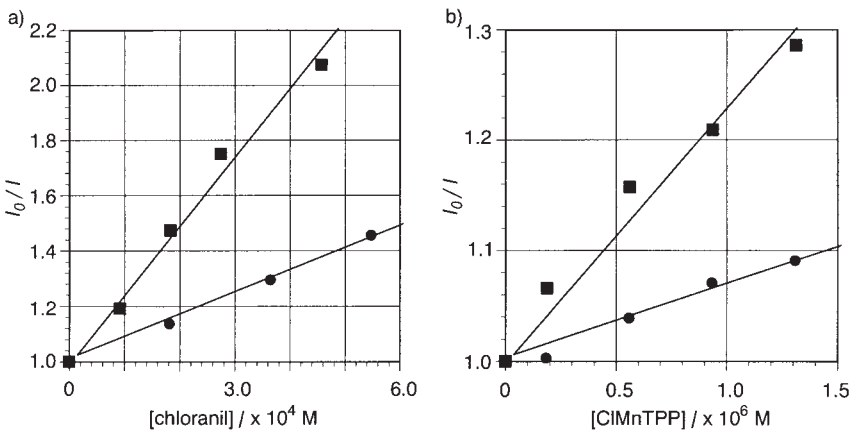

Fig. 8. Stern–Volmer plots for **9** (1.6 μM, square) and **11** (1.6 μM, circle) with (a) chloranil and (b) ClMnTPP in toluene.

2.2 Formation of Antenna Liposome Made by Porphyrin Amphiphile as a Single Component. In nature, all the energy conversion systems are operated in a form embedded in the biological membrane. Any artificial photosynthetic system developed must finally be incorporated in the membrane in order to generate proton concentration gradient across the membrane. Incorporation of the system into a membrane may also be important to elucidate the effect of environment and to increase the energy conversion efficiency, if any. In the research in this section, porphyrin itself was made amphiphilic and assembled into a form of liposome by combined intermolecular interactions of its own without assistance of any other lipid components. Therefore, the chromophores are positioned very closely to each other to afford the effective antenna function. For this purpose, we prepared bis(imidazolyl)porphyrin **12** having two *meso*-4-(*ω*-carboxyalkoxy)phenyl substituents (Scheme 6).[57]

Compound **12** was dispersed in water by sonication and subjected to gel filtration column separation to isolate the fraction corresponding to small unilamellar vesicles. The mean diameter of the vesicles was determined to be 27 ± 8 nm by dynamic light scattering (DLS) measurements. The aqueous sample was then applied on a smooth mica plate and dried in air. Figure 9 (a) shows a top view of the atomic force microscope (AFM) image and Fig. 9 (b) shows the side view along the line in (a). The observed full widths at the baseline level were 36, 32, and 38 nm for images (A), (B), and (C), respectively. These values are larger than those estimated from DLS measurements, due to the geometrical tip/sample convolution effect with tip curvature radius of 10 nm. However, a TEM image of the liposome dispersions shown in Fig. 9(c) revealed many particles of diameters in the range 20–30 nm, corresponding to the size distribution obtained by the DLS measurement.

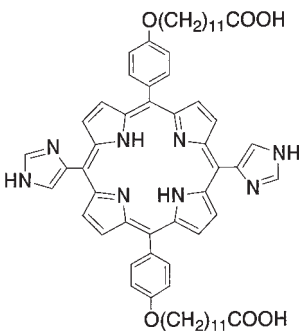

12

Scheme 6. Structure of bis(4-imidazolyl)-bis[4-(*ω*-carboxyalkyloxy)phenyl]porphyrins **12**.

The size of the system is larger than that of spherical micellar aggregates of the conventionally observable range 2–4 nm[70,71] and in accord with a typical range for small unilamellar vesicles: 20–30 nm. The presence of an interior aqueous phase and the capacity to keep polar solutes inside the vesicle were confirmed as follows: a hydrophilic fluorescent probe pyranine was cosonicated with **12** and the dispersion was isolated by a Sephadex G-50 gel filtration as above.[72] Because of the strong absorption of porphyrin **12** and the diffraction from the vesicle dispersion, no absorption of pyranine could be detected in the UV-vis spectrum. However, the presence of pyranine in the fraction from a gel filtration column was detected by its fluorescence spectrum, as shown in Fig. 10 (a). The initial fluorescence intensity of pyranine was low, due to the self-quenching inside liposome that reflects

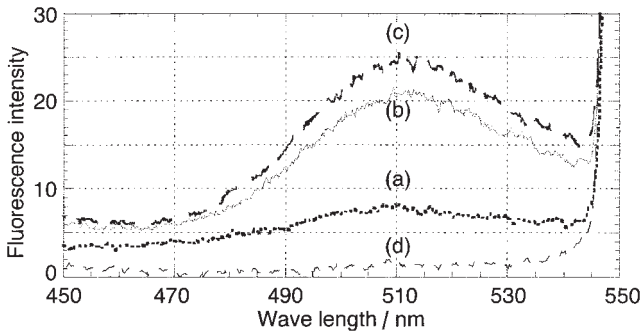

Fig. 10. Fluorescence spectra of porphyrin dispersion cosonicated with pyranine, $\lambda_{EX} = 280$ nm. (a) Just after gel filtration (Sephadex G-50); (b) the same after 24 h and (c) 40 h; (d) same as (a) without cosonication, but after treatment with 0.3 mM pyranine, followed by gel filtration.

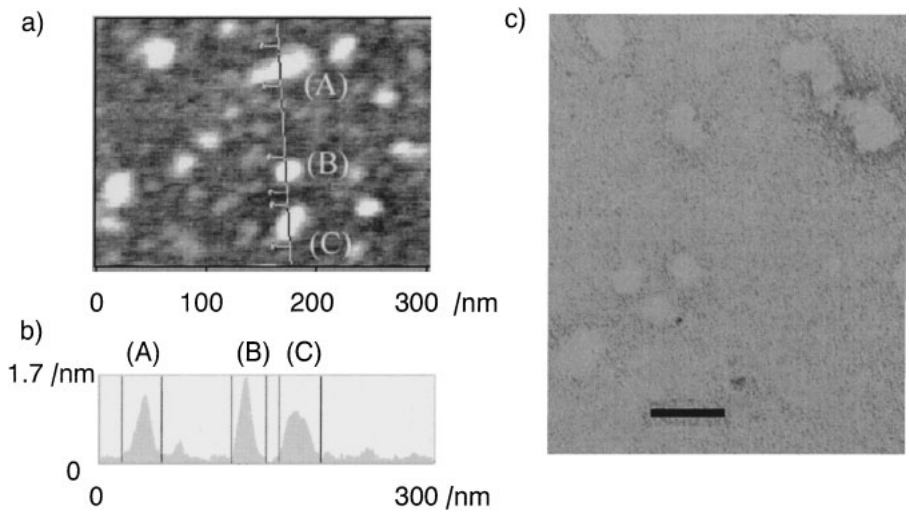

Fig. 9. AFM image of dispersion prepared from **12** developed on mica. a) A top view and b) a cross-section along the line in a), c) TEM image of negatively stained samples of dispersion from **12** with uranyl acetate (bar = 50 nm).

the relatively high initial concentration of 0.3 mM. Figures 10 (b) and (c) show the emission from pyranine after 24 h and 40 h, respectively, from the gel filtration column separation. The intensity gradually increased by the release to outside in a slow time-course and reached a saturation value after 40 h.

In a separate experiment, similarly prepared liposome was broken by the addition of 0.1 mL of 0.1% aqueous solution of Triton X-100 and the fluorescence intensity of pyranine was increased three times. It may be safely concluded that pyranine has been entrapped in the internal aqueous space. An opposing discussion may still claim that pyranine could be adsorbed on the membrane surface of liposome, although it is unlikely considering that both pyranine and membrane surface are negatively charged. In order to exclude this possibility completely, the liposome was once prepared without the addition of pyranine and then gel-filtrated. The liposomal fraction was immersed in a 0.3 mM pyranine solution and gel-filtrated again; no fluorescence emission of pyranine (Fig. 10 (d)) was observed from the liposome fraction. The combined results clearly prove that pyranine is entrapped in the interior space of liposome and is released slowly to the exterior through the membrane to emit fluorescence now liberated from the concentration quenching.

A schematic representation of the liposome formation from **12** is shown in Fig. 11. It is noteworthy that the liposomes are made only of bis(imidazolyl)porphyrin **12**, without any phospholipid such as lecithin. To the best of our knowledge, only Fuhrhop and co-workers reported one example of liposome formation from porphyrins in the literature.[73] In their report, tetrakis[*o*-(bixinylamino)phenyl]porphyrin was stabilized by side chain polymerization. In our system, the primary driving force for the formation of membrane aggregates comes from formation of a hydrogen-bonding network of imidazolyl substituents combined with hydrophobic and ionic interactions of the amphiphilic porphyrin in aqueous solution.

The Soret band of **12** dispersed in water ($\lambda_{max} = 426$ nm and hbw = 91 nm) resembled that of **9** in cyclohexane ($\lambda_{max} = 432.5$ nm and hbw = 86 nm). Both Soret bands were significantly red-shifted and broadened compared to that of **9** in methanol ($\lambda_{max} = 417$ nm and $hbw_{Soret} = 40$ nm). As mentioned above, **9** assembled into primarily a slipped cofacial orientation (Type A) along with some head-to-tail contribution (Type B) through imidazole–imidazole hydrogen bonds in non-polar solvents such as cyclohexane, toluene or $CDCl_3$, but not in methanol. Similar structure formation is reasonably expected for the dispersion of **12** in water by hydrogen bond networks in the aggregate assembled by hydrophobic interactions. A further stabilization may be provided by π–π interactions of porphyrins assembled in the central part of the membrane and therefore favored by an entropy term. The symmetrical structure of two (ω-carboxyalkoxy)-phenyl-substituted porphyrin may not be ideal for the formation of liposomes of small curvatures. However, a membrane-penetrating lipid, dialkylglycerol tetraether from thermophilic archae bacteria,[74] provides a convincing example of stable liposome formation from such symmetrical transmembrane lipids. The liposome obtained solely from porphyrin amphiphiles is regarded as a huge antenna. This may provide interesting materials for testing various functions such as light harvesting, light-induced charge separation, and electron transfer across the membrane.

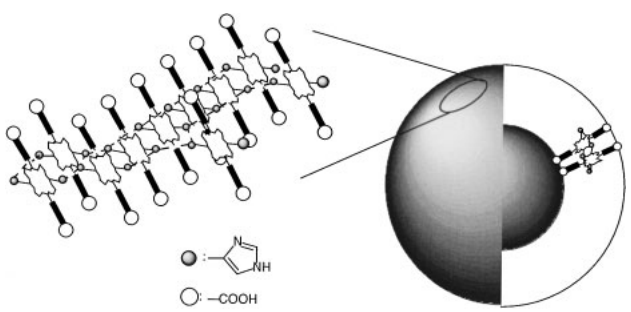

Fig. 11. Schematic representation of the liposome structure of **12** in aqueous solution.

3. Self- Assembly by Coordination to External Metal ion by Chelation

3.1 8-Hydroxyquinolyl Substituted Porphyrins. In section 1, we have explained the possibility of assembly formation by using coordination of a monodentate ligand to the central metal ions. If one tries to find metal ions other than the porphyrin center, there are many possible candidates. Most porphyrin assemblies discussing here are focused on antenna functions and therefore metal ions having an open shell electronic structure are eliminated. Chelating ligands are of special importance because of large stability constants and rigid structure formation. As one of the best combinations satisfying the above condition, we have chosen here a Ga-oxinate combination. Oxine (8-hydroxyquinoline) is known to form extremely stable, neutral, and rigid complexes with various metal ions such as Al(Ⅲ) and Ga(Ⅲ).[75,76] Further, tris(oxinato)Al(Ⅲ) and -Ga(Ⅲ) are known as organic light-emitting diodes (OLED),[77,78] and therefore these are expected to assist efficient energy transfer.

5-(8-Hydroxy-5-quinolyl)-porphyrin **13** and 5,10-bis(8-hydroxy-5-quinolyl)-porphyrin **14** were designed as precursors for porphyrin assemblies. Porphyrin **13**, whose 8-hydroxy-5-quinolyl group was attached directly to the *meso* position, was expected to afford a rigid gallium-tris(porphyrin) complex **15** like a pinwheel as shown in Scheme 7. This minimum unit can be extended to a dendritic structure **16** by the introduction of another 8-hydroxy-5-quinolyl group into porphyrin, as illustrated in Scheme 7.

Tris(porphyrinyl-oxinato)Ga(Ⅲ) complex **15** was synthesized from mono(8-hydroxy-5-quinolyl)porphyrin **13** (3 equiv) and $GaCl_3$ (1 equiv). UV-vis spectra of the starting monomer **13** and its Ga-complex **15** are shown in Fig. 12. The absorption band from the 8-hydroxy-5-quinolyl part appearing at 250 nm for the monomeric species **13** was shifted to 264 nm on the Ga complex in **15**. The Soret and Q-bands of **15** appeared at 425 nm and at 520, 555, 595, and 654 nm, respectively. These absorption bands were almost identical with those of monomeric species **13**, being 423 (Soret) and 519, 555, 595, and 653 nm (Q-bands). A small change was observed only for the half bandwidths of the Soret band, which are 26 and 18 nm for **15** and **13**, respectively. The molecular weight of **15** was determined by vapor-pressure osmometry in $CHCl_3$ solution (8.9×10^{-4} M) as 2105, the value corresponding to the tris(oxinato) complex (Calcd 2235) within the associated errors. The ^{1}H NMR spectra (1D, H–H COSY, and variable temperature) of **15** referring to tris(oxinato)Ga(Ⅲ) established a *meridional* form. Molecular mechanics calculation

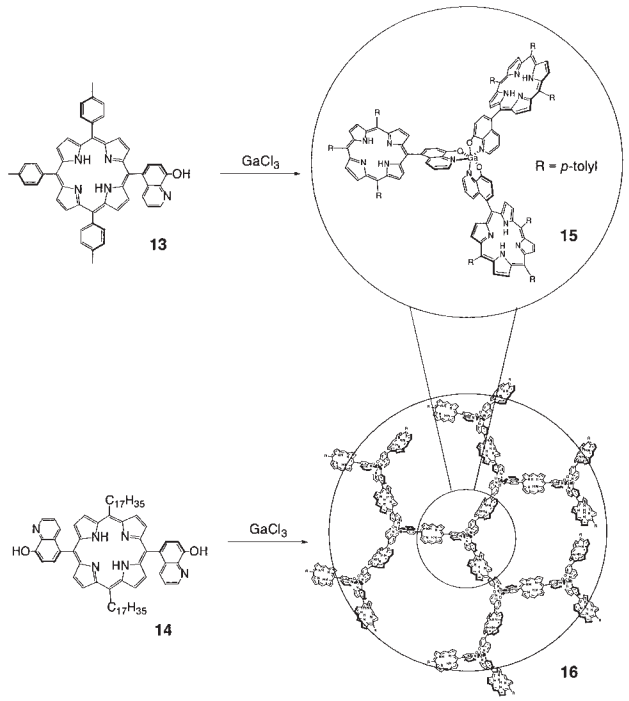

Scheme 7. Mono(oxinyl)porphyrin **13**, bis(oxinyl)porphyrin **14**, and their tris(oxinato)Ga(Ⅲ) complexes **15** and **16**.

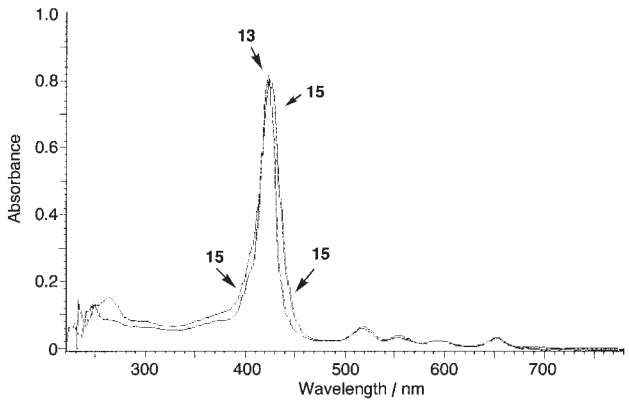

Fig. 12. UV-visible absorption spectra of (8-hydroxy-5-quinolyl)porphyrin **13** and its Ga complex **15** in $CHCl_3$.

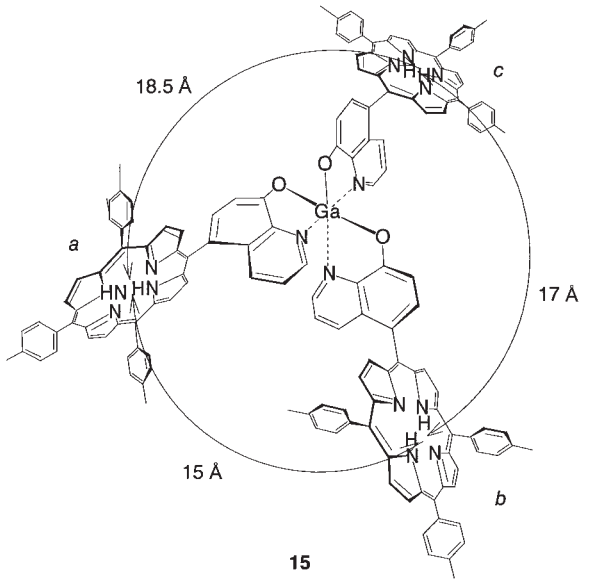

Fig. 13. Center-to-center distances of three porphyrins estimated by molecular mechanics calculation by using an MM + force field.

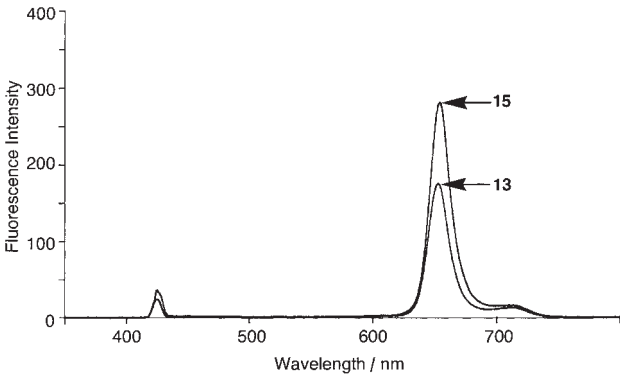

Fig. 14. Fluorescence spectra of **13** and **15**, whose maxima appeared at 652 and 712 nm, and 654 and 712 nm, respectively. Excitation at 423 and 425 nm for **13** and **15**, respectively.

(with MM + force field) deduced the most stable configuration as shown in Fig. 13 and the center-to-center separation distances between the three porphyrin units were estimated as 15, 17 and 18.5 Å for *a*–*b*, *b*–*c*, and *c*–*a*, respectively.

Fluorescence from tris(oxinato)Ga(Ⅲ) as the reference compound appeared at 529 nm when excited at 398 nm, but no peak could be detected in this region for **15**. Efficient energy transfer from (oxinato)Ga to porphyrin parts of lower excited energy levels may account for this observation. It is interesting to note that the fluorescence intensity of **15** is significantly larger than that of **13**, by a factor of 1.5 (Fig. 14). The fluorescence lifetime was estimated as 8.6 ns for **15** in a CH_2Cl_2 solution. This value was almost same with those of the monomeric species, 8.8 ns for **13** and 8.7 ns for tetra(*p*-tolyl)porphyrin. Absorption and fluorescence spectral data suggest that the electronic state of porphyrin unit in the complex is not perturbed significantly either by intramolecular porphyrin-porphyrin interactions, by Ga complexation or by introduction of the 8-hydroxy-5-quinolyl unit.

The quenching of the steady-state fluorescence of **15** by *p*-benzoquinone (BQ) is ~2.3 times more efficient than that of **13**, as found by analyzing Stern–Volmer plots as shown in Fig. 15 (inset). The dependence of the diffusion rate constant k_d on the size of the reactants could be estimated by $k_d \approx (R_a + R_b)^2/(R_a R_b)$, where R_a and R_b are the radii of the reactants (in the spherical model). This relation suggests that, if the size of one reactant (BQ) is much smaller than that of another reactant (excited **13** or **15**), the diffusion rate should be scaled proportionally to the size of the large reactant. In the present case, the estimated diffusion rate should increase by a factor of ~2 from the monomer (**13**) to the complex (**15**). This value is similar to that observed experimentally, supporting the idea of an efficient energy transfer between the porphyrin units in the complex.

In order to determine the energy-transfer rate between the porphyrin units in the complex directly, we measured time-

resolved anisotropy. The fluorescence decays with fluorescence polarized parallel ($I_{\parallel}(t)$) and perpendicular ($I_{\perp}(t)$) to the plane of the excitation light were measured for **13** and **15**. The fluorescence anisotropy ($r(t)$) was calculated by the following equation:

$$r(t) = (I_{\parallel}(t) - I_{\perp}(t))/(I_{\parallel}(t) + 2I_{\perp}(t)) \quad (1)$$

The anisotropy decays and analyses of **13** and **15** measured at 720 nm are shown in Fig. 15 and Table 4, respectively. The anisotropy decay of **13** simply reflects the rotational dynamics of porphyrin. From the simple Stokes–Einstein law, we can expect the average rotational time constant of the whole porphyrin molecule to be ~100 ps. Two decay components could be expected, corresponding to the in-plane rotation of the porphyrin (fast component) and that around the axis located in the porphyrin plane (slow component). The average rotational time of complex **15** was estimated to be ~1 ns. The actual anisotropy decay of the complex **15** contained a component much faster than that of monomer **13** (Fig. 15 and Table 4). Three-exponential fit with a fixed slow-decay component of 800 ps gave a fast component of ~10 ps, assignable to the energy transfer between the closest porphyrin units in the complex. The second component of 86 ± 20 ps is still too fast to assign for the rotational motions of the complex and probably reflects an energy-transfer process between the porphyrin units, which are located farther from each other. These data suggest that the energy-transfer between the porphyrin units in the complex **15** is repeated roughly ~800 times within its lifetime of 8.6 ns.

Dendritic oxinato-porphyrin complex **16** was synthesized by adding an ethanol solution of gallium(Ⅲ) chloride into a chloroform solution of **14**. Since the resulting film of **16** was insoluble in any organic solvents, absorption and fluorescence spectra of the film on glass plate were measured with an optical microscope. UV-vis spectra of film-like samples **14** and **16** are shown in Fig. 16. Uniform areas (0.2 mm × 0.3 mm) were observed for both samples, and the sample from **14** was adjusted so that its Soret band had similar absorbance. The Soret band of **16** was slightly shifted to a longer wavelength, and the half bandwidth of the Soret band of **16** spread into 42 nm from 34 nm for the case of **14**. The Q-bands were almost identical with those of monomeric species **14**.

Fluorescence spectra at the same areas for the above two samples were also obtained, as shown in Fig. 17. No fluorescence from the oxinato-Ga part (529 nm) could be observed in this case also. Fluorescence from the porphyrin part seems to be increased significantly by complexation in this case too, with an increased factor of 2.2 (= **16/14**). Therefore, the fluorescence was even intensified by the formation of dendritic porphyrin structure rather than conventionally observable quenching phenomina on assembly formation. The assembly is interesting as a unique material to accommodate the part of charge separation site in the membrane phase. In order to construct the whole photosynthetic composite, donor and acceptor could be incorporated in the membrane or added to outer or inner aqueous phases.

3.2 Bipyridyl Substituted Porphyrin. The next topic is control of molecular orientation by complexation reaction between chelate ligand and metal ion, leading toward a molecular switch. The orientation of the two porphyrin directly linked by a chelating substituent should depend on the geometry around chelated metal ion. Such a bisporphyrin would be applicable as a molecular switch[79,80] and would be of use in molecular devices

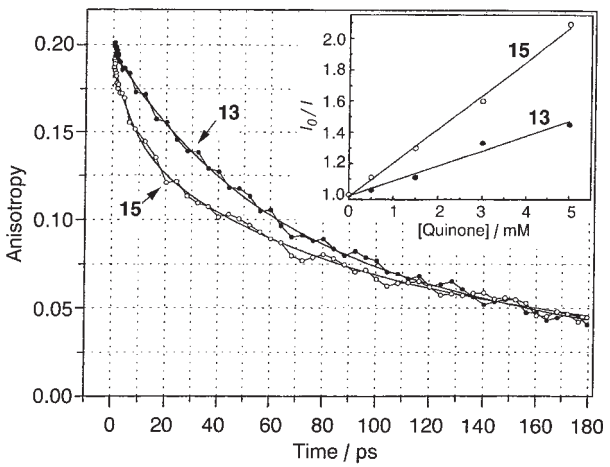

Fig. 15. Decay of the fluorescence anisotropy at 720 nm for monomer **13** and complex **15** in CH_2Cl_2. Inset: Stern–Volmer plot for the quenching of the fluorescence intensity of **13** (1.5 mM) and **15** (0.5 mM) by *p*-benezoquinone.

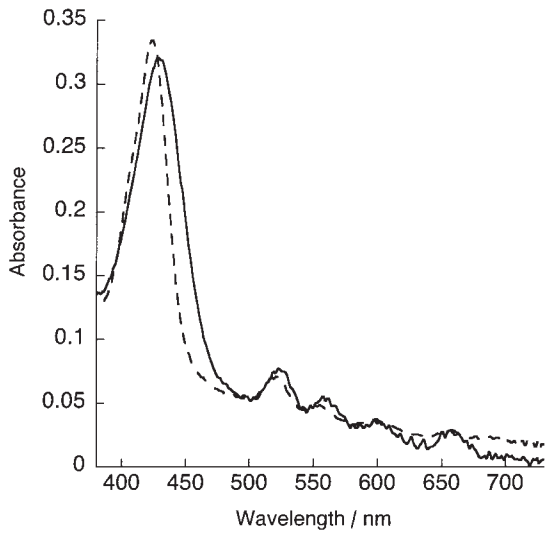

Fig. 16. UV-vis spectra of film-like samples of monomeric porphyrin **14** (broken line) and Ga-porphyrin assembly **16** (real line) on glass plate.

Table 4. Analyses of Fluorescence Depolarization Decay in CH_2Cl_2

Compound	τ_1 / ps	A_1	τ_2 / ps	A_2	τ_3 / ps	A_3
15	9 ± 3	0.047 ± 0.007	86 ± 20	0.102 ± 0.005	800	0.042 ± 0.002
13	49 ± 5	0.096 ± 0.003	203 ± 20	0.1		

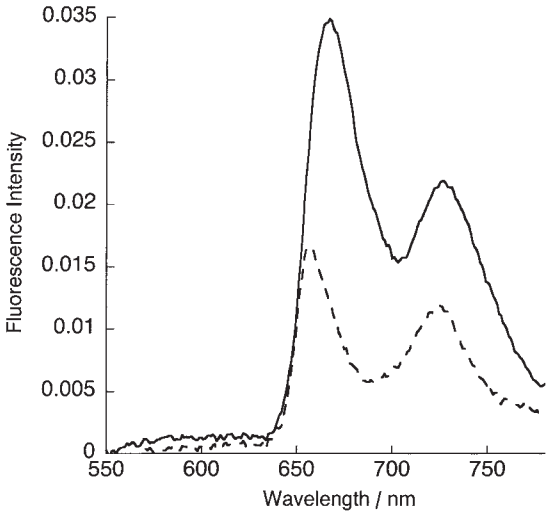

Fig. 17. Fluorescence spectra of film-like samples of monomeric porphyrin **14** (broken line) and Ga-porphyrin assembly **16** (real line) on glass plate. The same areas of the above samples (Fig. 16) were measured. Excitation at 400–440 nm with a band-path filter.

and molecular machines.[81–83] Therefore porphyrin dimer **17**, in which two porphyrin units were connected directly to 4,4′-positions of the bipyridyl group, was designed and synthesized by using a nickel-mediated coupling reaction of monomeric bromopyridinylporphyrin **20**.

In our first trial, one-step introduction of two porphyrin units by condensation of 4,4′-diformyl-2,2′-bipyridine and octanal with dipyrromethane was unsuccessful (Scheme 8A). In this case, little desired bisporphyrin was obtained. Therefore, a homocoupling reaction of bromopyridinylporphyrin **20** was examined (Scheme 8B). Nickel(0)-mediated coupling reaction of aryl halides normally proceeds under mild conditions, and many successful preparative examples of biaryl compounds are reported.[84–86] To our best knowledge, however, no synthesis of porphyrin derivatives by nickel(0)-mediated homocoupling reaction has been reported; therefore, a simple and efficient strategy for the synthesis of **17** was explored. After optimization of various reaction conditions, the best result was obtained by the use of a large excess of $[Ni(cod)_2]$ (ca. 25 equiv) in the presence of 2,2′-bipyridyl (1.3 equiv) and cyclooctadiene (ca. 30 equiv) with use of 6.6×10^{-4} M of **20** in dry DMF. The starting material **20** was completely consumed within 24 h, and the desired bisporphyrin **17** was obtained as the major product. Pure bisporphyrin **17** was isolated with axial coordination of pyridine (from eluent of GPC separation) in a 58% yield with consistent NMR data. The ^{1}H NMR spectrum of **17** (20 μM in $(CDCl_2)_2$) is shown in Fig. 18A. All protons could be assigned by using H–H COSY and TOCSY spectra. Protons of the axial pyridines, PyH_2, PyH_3, and PyH_4, were significantly shielded by porphyrin rings and appeared at 3.5, 5.8, and 6.6 ppm, respectively. In order to switch the environment of porphyrin moieties, the complexation behavior of **17** was monitored by NMR spectrometry after the addition of palladium(II) chloride. After the addition of 1.1 equiv of $[PdCl_2(CH_3CN)_2]$, new signals appeared at 9.9, 9.5, 8.8, 8.5, 7.8, 7.3, 4.8, and 2.4 ppm (indicated as arrows in Fig. 18C), and the signals of **17** (9.6, 9.0, 8.1, 5.0, and 2.5 ppm) were gradually

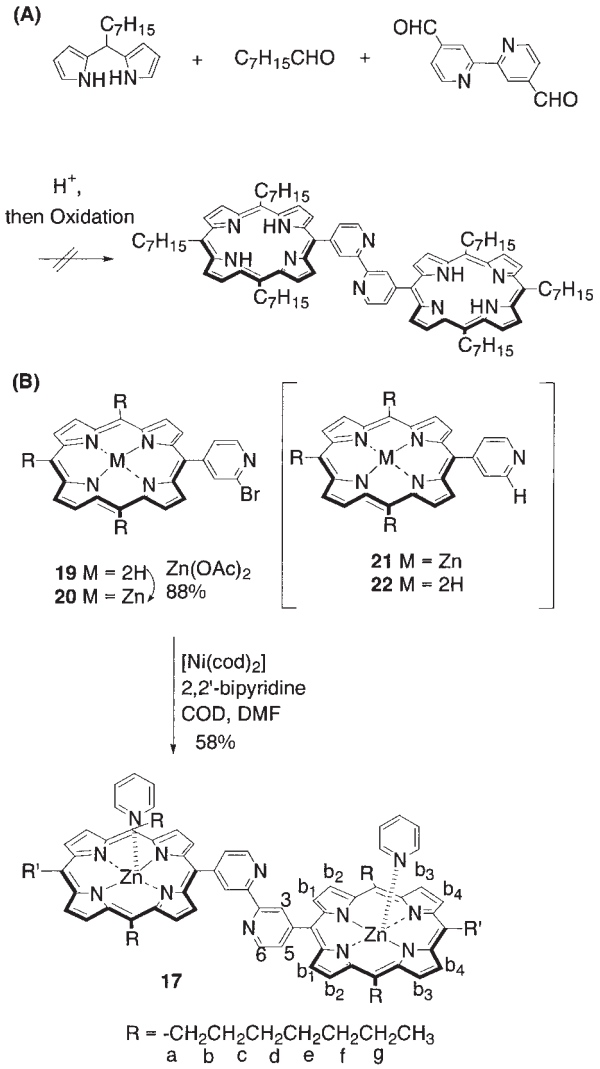

Scheme 8. Two synthetic routes of bipyridyl-bridged bisporphyrin; (A) directly from 4,4′-diformyl-2,2′-bipyridyl; (B) Ni(0)-mediated coupling reaction.

reduced. After the addition of 2.2 equiv of $[PdCl_2(CH_3CN)_2]$, the spectrum turned completely to that of the palladium complex **18** (Scheme 9) along with the $[PdCl_2(pyridine)_2]$ complex (Fig. 18D). Protons of **18** could also be assigned by H–H COSY and TOCSY spectra. The large downfield shift of H_6 (+0.9 ppm) reflects the development of partial positive charge on complexation with $PdCl_2$. The most sensitive shielding effect of porphyrin ring current appeared at the H_3 proton (−0.6 ppm). According to the symmetry, there are two *meso*-heptyl groups in porphyrin **17**, opposite and adjacent *meso* positions with respect to the bipyridyl group in a 2:1 ratio. Before complexation, however, they were not distinguishable in the ^{1}H NMR spectrum because of free and rapid rotation along the bond connecting two pyridyl units. When palladium complex **18** was formed, H_a and H_b in two heptyl groups around at 4.8 and 2.4 ppm were split into 4.80 and 4.85, and 2.36 and 2.42 ppm, respectively. The peak separation between two heptyl groups at the opposite position, R′, and four at the adjacent, R, is now detectable because of different distances from the facing porphyrin plane. These results show that the addition of 2.2 equivalents of Pd(II) completely converts the compound from

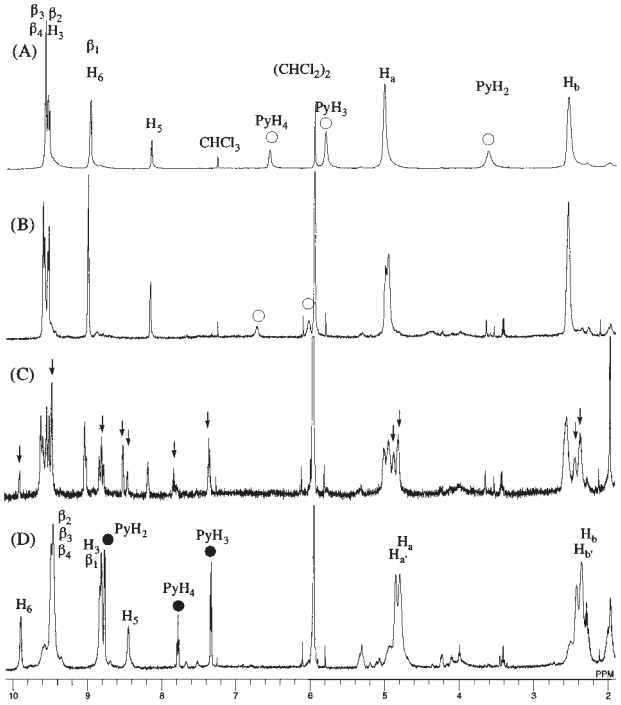

Fig. 18. ^{1}H NMR titration of **17** with $PdCl_2$ (600 MHz, in $(CDCl_2)_2$). (A) **17** (20 μM), (B) **17** (1.6 μM), (C) (B) + 1.1 equiv $[PdCl_2(CH_3CN)_2]$, (D) (B) + 2.2 equiv $[PdCl_2(CH_3CN)_2]$. Open circle; coordinated pyridine, filled circle; $[PdCl_2(pyridine)_2]$.

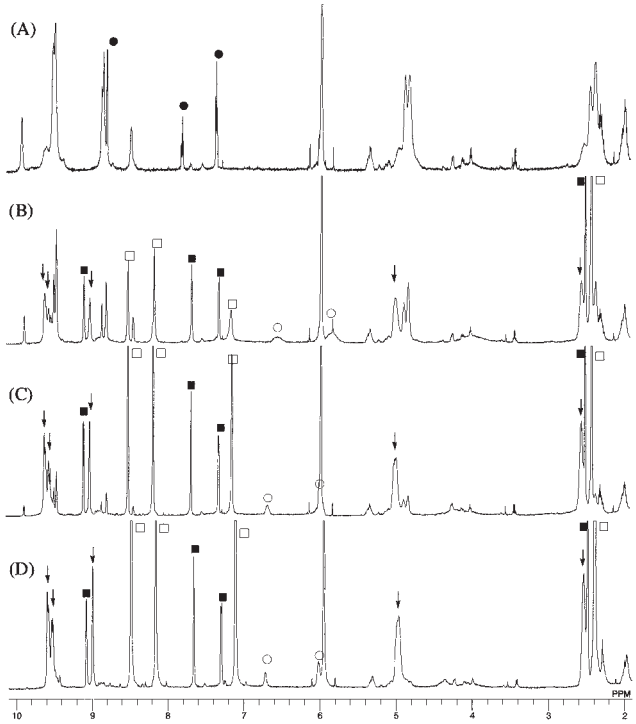

Fig. 19. ^{1}H NMR titration of **18** with 4,4′-dimethyl-2,2′-bipyridine (600 MHz, in $(CDCl_2)_2$). (A) **18** (1.6 μM, the same spectrum as Figure 18D), (B) (A) + 4,4′-dimethyl-2,2′-bipyridine (1.3 equiv), (C) + 2.7 equiv, (D) + 6.8 equiv, open circle; coordinated axial pyridine, filled circle; $[PdCl_2(pyridine)_2]$, open square; 4,4′-dimethyl-2,2′-bipyridine, filled square; 4,4′-dimethyl-2,2′-bipyridine-$PdCl_2$ complex.

a freely rotating conformation to an open-mouth one, even at such an extremely dilute solution as 1.6 μM.

In order to switch the cofacial conformation of bisporphyrin **18** back to the original bipyridyl porphyrin **17**, 4,4′-dimethyl-2,2′-bipyridine was added to the mixture. The reaction course was monitored by ^{1}H NMR spectroscopy (Fig. 19). When 1.3 equiv of bipyridine were added, signals of $PdCl_2$(pyridine)$_2$ at 8.8, 7.8, and 7.4 ppm (filled circle in Fig. 19A) disappeared completely with appearance of signals of coordinating pyridines at 6.5 and 5.8 ppm (open circle in Fig. 19B). On further addition of bipyridine, signals of palladium complex **18** were decreased, and the signal of uncomplexed **17** (indicated as arrows) increased in contrast. Finally, the addition of 6.8 equiv of bipyridine eliminated almost all the signals of **18**; signals of **17** (arrows), 4,4′-dimethyl-2,2′-bipyridine-$PdCl_2$ complex (filled squares), and free 4,4′-dimethyl-2,2′-bipyridine (open squares) were observed (Fig. 19D). These results are summarized in Scheme 9, where reversible complexation of the bipyridyl part with $PdCl_2$ controls the orientation of two porphyrins along with the axial ligation of pyridines.

4. Self-Assembly by Successive Coordination to Two Metal Centers

4.1 Formation of One-Dimentional Porphyrin Array. As described in section 1.1, we have introduced an idea of complementary coordination of imidazolyl to pentacoordinating Zn(II) to form a slipped cofacial porphyrin dimer **3**, which showed an extremely large stability constant of over 10^{10} M^{-1}. Combination of imidazolyl and Zn(II) in porphyrin gave an ideal unit to lead to a multi porphyrin array by stable complementary coordination. In order to obtain higher supramolecules, we have prepared bis(*N*-methyl-2-imidazolylporphyrinatoZn) **24** which

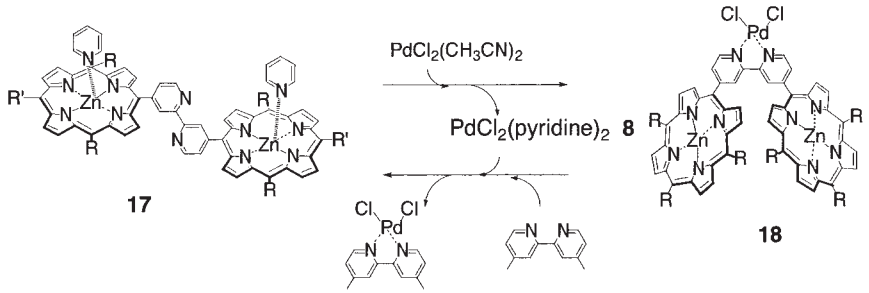

Scheme 9. Reversible conversion between **17** and **18**.

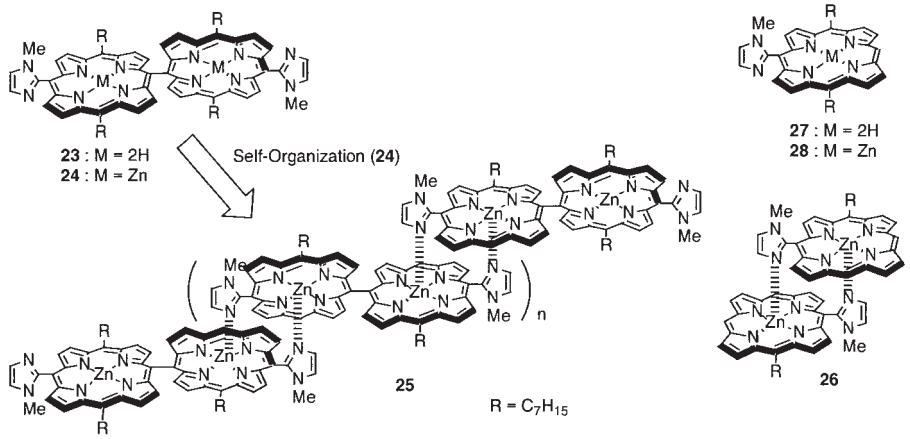

Scheme 10. Formation of one-dimensional giant porphyrin array by complementary coordination of imidazolyl to zinc.

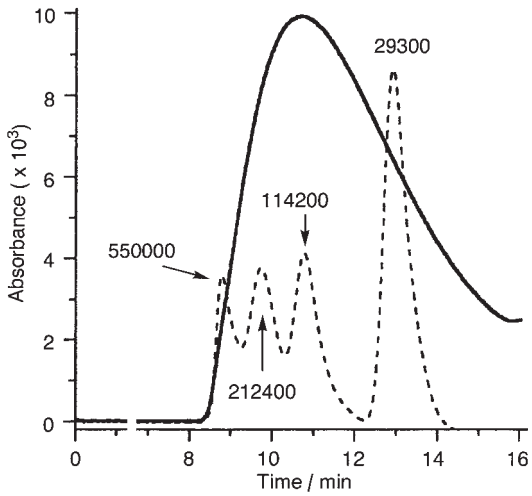

Fig. 20. GPC chart of **25** (bold line) and standard polystyrene mixtures (dotted line, the numbers indicate molecular weight) with a column of exclusion limit 5×10^5. The eluent is EtOH-free $CHCl_3$.

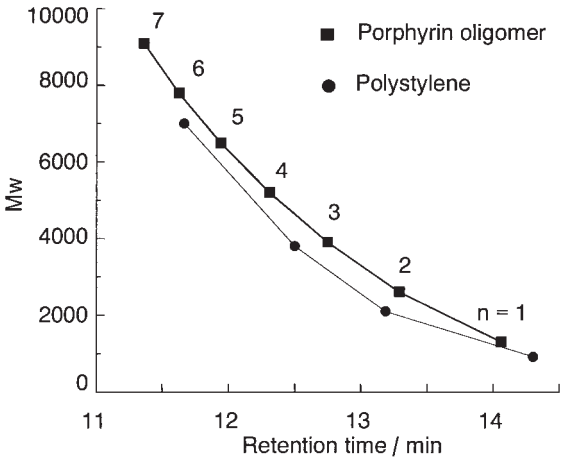

Fig. 21. GPC calibration curve of self-assembled porphyrin oligomer from the data of Fig. 24 (bold line) and standard polystyrene mixtures (dotted line, the numbers indicate molecular weight) with a column of exclusion limit 5×10^5. The eluent is EtOH-free $CHCl_3$.

was directly linked at *meso*-positions[41] by the direct oxidative coupling reaction developed first by Osuka.[29,37,87–90] Complementary coordination independently at two imidazolylporphyrin units with an orthogonal orientation of the π-orbital planes led to the formation of linear multi-porphyrin array **25** (Scheme 10).

The molecular weight of **25** was analyzed by using gel permeation chromatography (GPC). Figure 20 illustrates chromatograms of **25** along with those of polystyrene standard mixtures. The elution of **25** started even before the standard of MW 5.5×10^5 by using the column having an exclusion limit of MW 5×10^5 and the peak maximum appeared around MW 1×10^5, which corresponded to the assembly of ca. eighty bis(imidazolylporphyrin) units (MW = 1298) through imidazole–Zn coordination bonds. Calibration plots of porphyrin oligomers prepared from the data of Fig. 24, which will be discussed below, and the data of polystyrene shown in Fig. 21 indicates that the porphyrin oligomers in this study should possess ∼1.3 times larger molecular weights than the polystyrene standards in GPC, and that the molecular weights discussed here may even give a low estimate. Since the molecular length of the repeating unit is estimated as 1.43 nm by MM calculation by using Cerius2, the molecular length of the porphyrin array reaches to 550 nm at its longest and to 110 nm at the distribution peak.

Figure 22 compares the absorption spectrum of **25** with those of free base **23** and zinc complex **26** in chloroform. The Soret bands of *meso*-linked dimeric species were split into twin peaks at 415 and 453 nm for free base **23** and 412 and 490 nm for Zn complex **25**. The splitting behavior can be explained by assuming two modes of exciton interactions caused by *meso–meso* linking and coordination.[41]

The above-mentioned multi-porphyrin array having such a huge molecular weight has been obtained in EtOH-free chloroform; coordination organization depends on the solvent polarity. The effect of MeOH addition to a $CHCl_3$ solution was monitored by the absorption spectrum (Fig. 23). Addition of methanol reduced the splitting width of the Soret band as a result of an obvious blue shift of the longer Soret band passing through a clear isosbestic point at 478 nm and a smaller red shift of the shorter Soret band. On the addition of 30% MeOH, the shift reached almost the saturation point, where the splitting of 41 nm is similar to that of **23** and may correspond to that of the isolated *meso–meso* linked bisporphyrin. These results suggest that

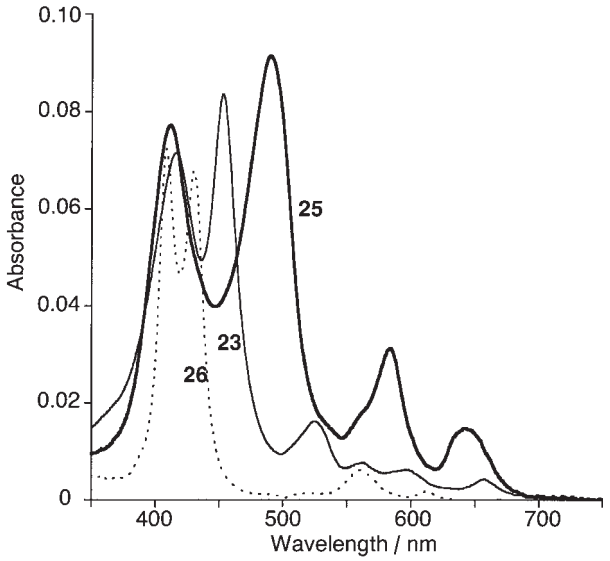

Fig. 22. Absorption spectra of bis(imidazolylporphyrin) free base **23**, bis(imidazolylporphyrinatozinc) array **25**, and imidazolylporphyrinatozinc **26** in $CHCl_3$.

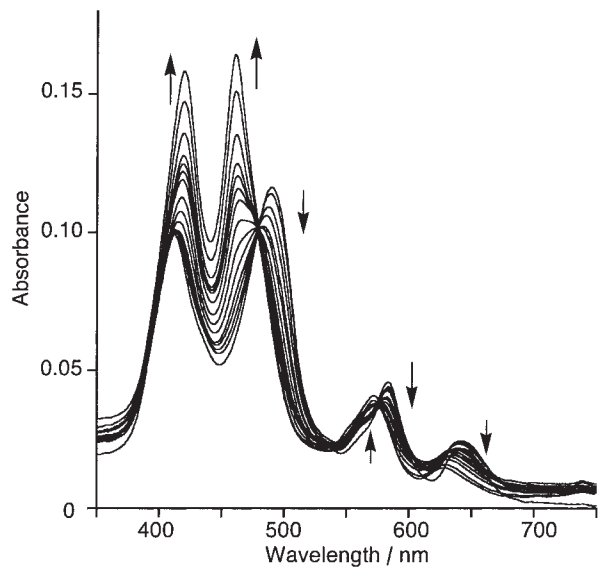

Fig. 23. Effect of the addition of MeOH to a $CHCl_3$ solution on absorption spectra of **25** (9.9×10^{-7} M). Each spectra was recorded after the addition of MeOH in the amounts 0, 1, 2, 3, 4, 5, 7, 9, 10, 12, 14, 16, 20, 25, and 30 volumes to 100 volume of a $CHCl_3$ solution of **25** according to the order of the arrow indicated.

MeOH competes with the imidazolyl coordination to zinc and that the addition of donating solvent such as MeOH can simply control the degree of organization.

A mixture of **26** and **25** in a 1:5 molar ratio in ethanol-free chloroform was analyzed by GPC with use of the column having an exclusion limit of MW 7×10^4 (Fig. 24). Two isolated peaks at 8 min (exclusion limit) and 14 min represent no scrambling between these components (solid line). Next, the same sample mixture was dissolved in a chloroform–methanol (1:1) mixture, followed by evaporation and subjection to GPC analysis (bold line). Then, many peaks of intermediate retention times appeared,

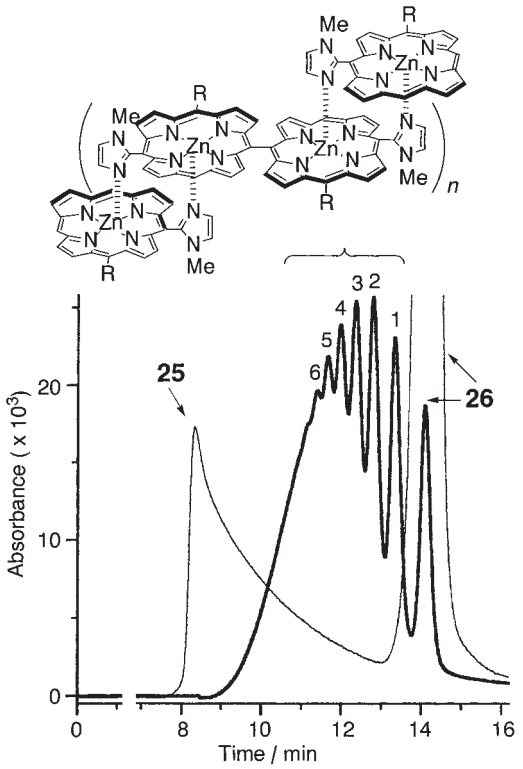

Fig. 24. GPC Chart of a mixture of **25** and **26** in a 5:1 molar ratio (solid line) and the same sample mixture once dissolved in $CHCl_3$–MeOH (1:1), then evaporated, and re-dissolved in $CHCl_3$ (bold line). The exclusion limits of the column employed was 7×10^4.

with a significant shift of the distribution maximum to a lower molecular weight. The peak at the longest retention time, 14 min, corresponds to **26**; peaks at shorter retention times, marked by 1, 2, 3, and more, are assigned as a series of compounds in which one unit of **24**, two, three and so on, are terminated by **28**'s at both ends. The results clearly demonstrate that the coordination-organized supramolecules can scramble in a mixed solvent of chloroform–methanol but not in ethanol-free chloroform in accord with the UV titration data and more importantly that the organization can also be controlled by the addition of an appropriate terminator such as **28**. When this terminator bears a thiolate group, it can afford the contact on gold surface for device applications. One example will be described in the next section.

4.2 Photocurrent Generation from One-Dimensionally Propagated Porphyrin Array on SAM. Recently, a self-assembled monolayer (SAM) of porphyrins on gold electrode was found to be an efficient method to convert light energy to electric current by photoinduced charge separation on the surface.[91–93] This approach limits the light absorption only to the single molecular layer and to the narrow absorption range of wavelengths, due to a sharp porphyrin Soret band (410–430 nm).[94,95] Since we have developed a unique methodology to obtain a giant porphyrin array by self-coordination of bis(imidazolylporphyrinatozinc) as mentioned in the above section, creation of a porphyrin monolayer fixed on the electrode surface by using Au–S bond was attempted to extend further into a sequential structure, which would bring about an increase of light absorption in the range of 350–750 nm.

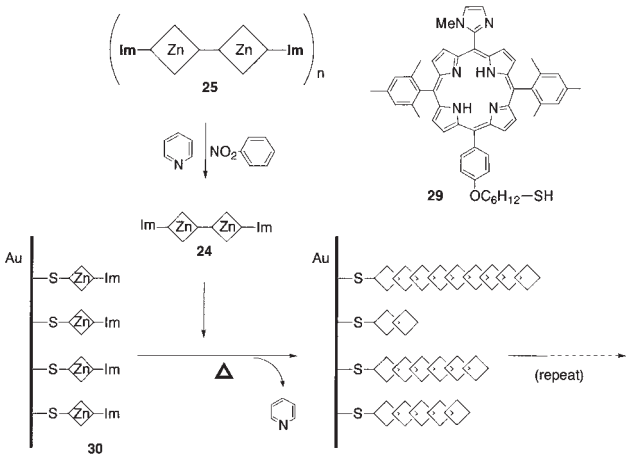

Scheme 11. Schematic representation of **29** and preparation of SAM **30**.

In order to apply the above principle, imidazolyl-appended porphyrin **29** bearing an ω-mercaptoalkyl substituent was prepared as the first layer molecule on the Au surface. SAM **30** was formed by soaking the Au electrode (1 cm × 3 cm) into a solution of porphyrin **29** (1.0 mM), followed by metal introduction by using a $Zn(OAc)_2$ solution ($CHCl_3$:MeOH = 10:1).[41] The surface concentration of porphyrin fixed on the Au electrode was estimated as 3.1×10^{-11} mol cm^{-2} from the anodic peak in the cyclic voltammogram.

Our strategy of sequential elongation of porphyrin is as follows. Compound **25** was dissolved in a 1:1 mixture of nitrobenzene–pyridine, where the multi-porphyrin array **25** was dissociated into monomeric unit **24** by competitive coordination of pyridine to the central Zn ion. An aliquot of this solution was applied dropwise to the electrode. Then pyridine was evaporated at 50 °C in a gentle stream of air for 10 minutes so that the multi-porphyrin sequence might grow on SAM **30** by the development of complementary coordination of imidazolyl to the central zinc (Scheme 11). Then another aliquot of porphyrin was applied and the accumulation procedure was repeated. The number of organized porphyrins (n) could be controlled by the concentration of **24** in the solution and the number of the above deposition cycles. AFM measurements showed long porphyrin assemblies extending from the surface of the electrode (Fig. 25). The absorption of visible light was obviously increased by the repeated deposition cycles.

Photocurrents were measured by irradiating the electrode plate of 0.5 cm^2 by a 150 W Xe lamp through an IR cut-off filter with application of negative bias voltage (−200 mV). The plate has been immersed in a 0.1 M Na_2SO_4 aqueous solution containing 5 mM methylviologen (MV^{2+}) as the electron carrier. The plot of photocurrent as a function of the irradiating wavelength, i.e. the action spectrum (Fig. 26), closely resembles the absorption spectra of porphyrin-assembled electrodes over the whole range of 350–750 nm. Photocurrent quantum efficiencies[96] at the respective absorption peaks were calculated as 0.14% (430 nm), 0.11% (490 nm), 0.10% (580 nm), and 0.26% (650 nm). These values are not large, but are reasonable if one considers that the system is composed only of simple porphyrins without incorporation of either electron donor or acceptor units.[97,98]

In Fig. 27, photocurrent values obtained by SAM **30** and electrodes (a)–(d) obtained along with other samples, are plotted

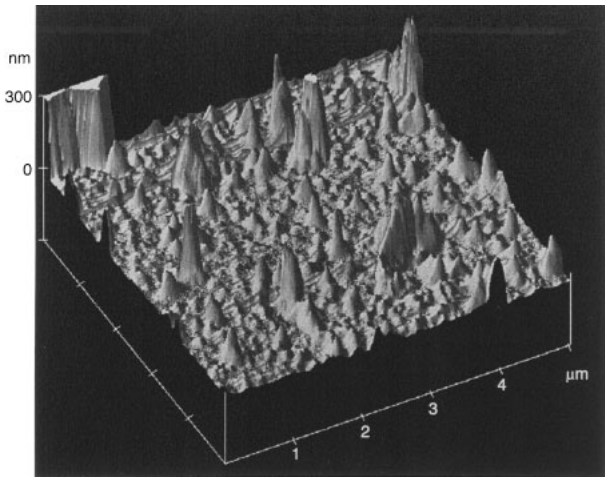

Fig. 25. AFM image of electrode (d) described in the legend of Fig. 27. Long porphyrin assemblies were observed to rise from many points on electrode (d). The heights are not homogeneous with an apparently broad distribution and some assemblies reach a few hundreds nanometer scale.

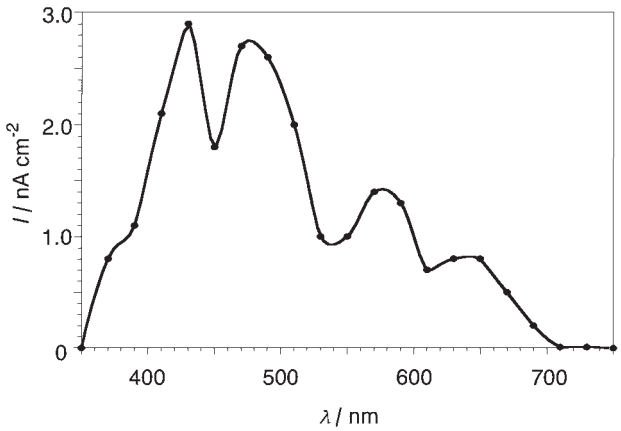

Fig. 26. Action spectrum of electrode (d) described in the legend of Fig. 27; 50 μW cm^{-2}, −200 mV vs Ag/Ag$^+$, under N_2, 0.1 M Na_2SO_4, 5 mM MV^{2+}.

as a function of the absorption area ($A\lambda$) integrated over the range of 350–750 nm. The current value increased uniformly with the increase of the absorption area, showing a sharp increase especially in the range 0–20 $A\lambda$. This increase reveals that the stalactite structure extended perpendicularly on the surface is of obvious advantage in the photocurrent generation. It is noteworthy that the photocurrent generation was improved simply by the porphyrin chain formation without incorporating any specific electron acceptor or donor groups. The increase comes primarily from the improved efficiency in the absorption of light energy and the excitation energy transfer by the accumulated porphyrins. Moreover, effective charge separation and electron/hole transfer along the multi-porphyrin chains may also be contributing.

4.3 Nonlinear Optical Property of Self-Assembled Porphyrin Array. There are several potential applications for self-assembled bis(imidazolylporphyrin) arrays. Third-order nonlinear optics (NLO) are one of the hopeful candidates along with the photocurrent generation, because NLO materials have

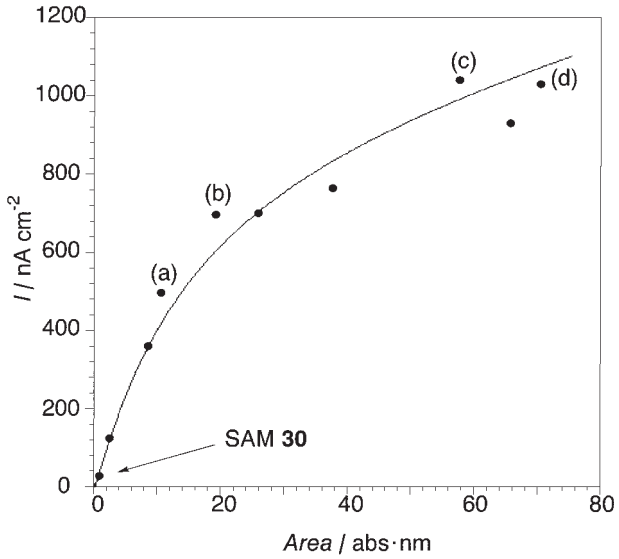

Fig. 27. Plot of photocurrent density of **30**, electrodes (a)–(d) and other electrodes as a function of the absorption area integrated over the range 350–750 nm (150 Xe lamp, under N_2). Concentration and repetition cycles are (a) 1 mM and once ($n = 2$), (b) 0.1 mM and three times, ($n = 4$) (c) 1 mM and three times ($n = 13$) and (d) 1 mM and four times ($n = 16$), respectively.

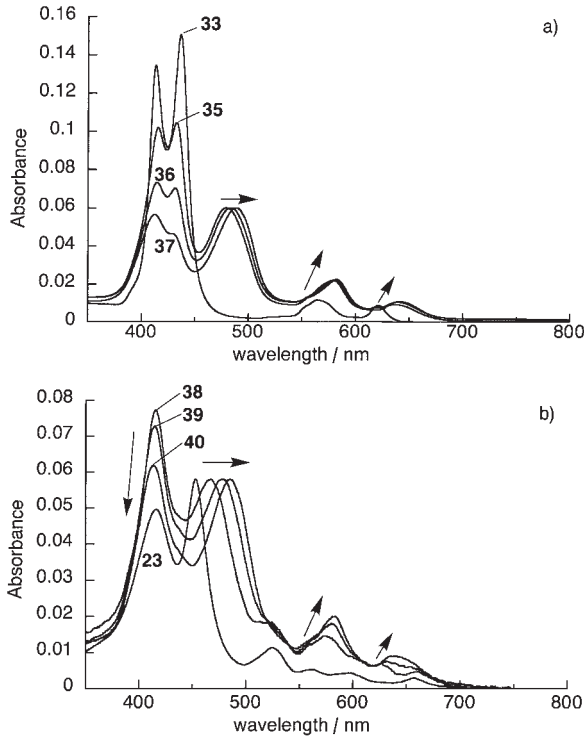

Fig. 28. a) Absorption spectra of isolated **33** and **35**–**37**, and b) **23** and **38**–**40** in $CHCl_3$. Concentrations were ~10 μM and absorbance was normalized at the split Soret band appeared at around 450 to 490 nm in each spectra. The shifted peaks at the longest wavelength of split Soret band were as follows: **35**; 480, **36**; 484, **37**; 489, **23**; 452, **38**; 467, **39**; 479, **40**; 485 nm.

potential utilities for photonic applications such as ultrafast optical switching and modulations.[19–21] It has been accepted generally that donor and/or acceptor terminal sets intervened by a π-conjugated system exhibit large $\chi^{(3)}$ values.[22–24] As described in section 4.2, the self-assembled bis(imidazolylporphyrin) array can be scrambled with other component porphyrins on applying dissociative conditions first, followed then by reorganization ones. By this procedure, specific donor and/or acceptor groups became available to be introduced at the molecular terminals of highly polarizable large π-electronic systems.

Porphyrin oligomers **35**–**37** and **38**–**40** were obtained by GPC separation from mixtures of **24** and **41**, and **24** and **34**, respectively, as shown in Scheme 12. Figures 28a and 28b compare the absorption spectra of isolated compounds, dimeric zinc-porphyrin **33**, **35**–**37**, and **38**–**40**, along with free base **23** in $CHCl_3$. The large splits of the Soret bands in the spectra that

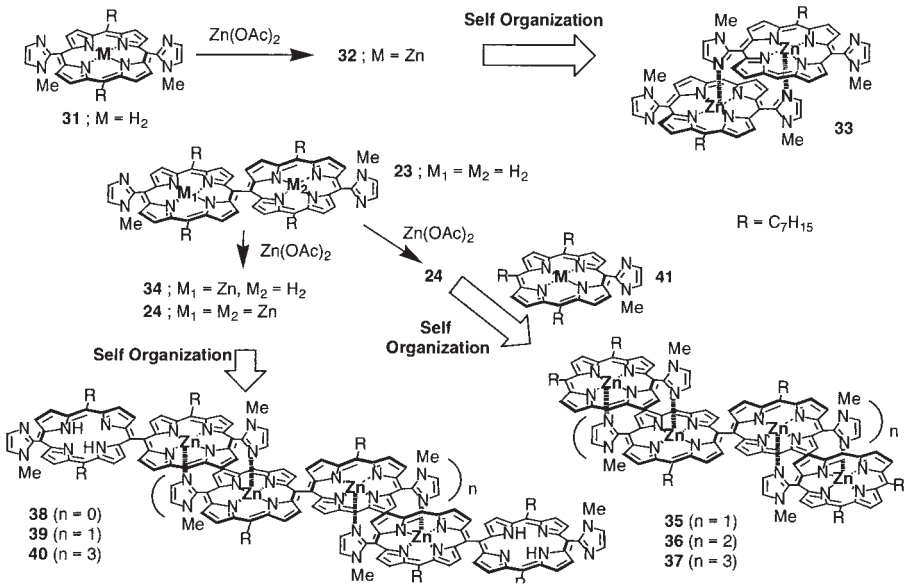

Scheme 12. Molecular structures and synthetic routes of porphyrins for NLO experiments.

Table 5. Nonlinear Optical Properties of Porphyrins by OKE Measurements

Porphyrins (No. of units)	$\lvert\gamma_{yyyy}\rvert$ 10^{-32} esu	γ_{real}/unit 10^{-32} esu	$\lvert\chi^{(3)}{}_{yyyy}\rvert$ 10^{-15} esu	$\chi^{(3)}{}_{real}$ 10^{-15} esu	Conc. 10^{-6} M
31 (1)	14		91		320
33 (2)	8		24		150
23 (2)	7		4		25
35 (4)	13		55		200
36 (6)	61		38		30
37 (8)	120		39		15
38 (4)	180	55	50	57	13
39 (6)	950	120	165	130	8.3
40 (10)	1300	150	163	150	5.0

appeared at around 410 and 450–490 nm originate from the exciton interaction by direct linking at *meso*-positions. As shown in the previous section, the longest wavelength of the split Soret band was sensitive to the degree of organization. The peaks shifted from 480 to 489 nm for the series of compounds, **35**–**37**, and from 453 to 489 nm for **23** and **38**–**40** with the increasing number of porphyrin units.

The femtosecond time-resolved optical Kerr effect (OKE) measurements were performed to evaluate the NLO property at off-resonant conditions at 800 nm. The results are summarized in Table 5. The orders of the polarizabilities $\lvert\gamma_{yyyy}\rvert$ and the susceptibilities $\lvert\chi^{(3)}{}_{yyyy}\rvert$ of oligomers **38**–**40** were extremely large, ranging from 10^{-30} to 10^{-29} esu and from 10^{-14} to 10^{-13} esu, respectively. On the other hand, the $\lvert\gamma_{yyyy}\rvert$ of the series of compounds **35**–**37**, which were terminated by monomeric zinc-porphyrin, were ranging from 10^{-31} to 10^{-30} esu. These were 10 times smaller than **38**–**40**. The method and conditions for previous reports of butadiyne-linked conjugated (DFWM, 45 ps laser) and *meso*–*meso* coupled (*z*-scan, 30 ps laser) porphyrin oligomers are not identical and direct comparison of our results with these data is difficult, but the compounds **38**–**40** exhibited large polarizabilities with a clear tendency to enhance the increments with the chain length.

Recently, some organic compounds, which were measured and analyzed under conditions similar to those of our study, i.e. OKE technique with fs pulse laser at off-resonant and CS_2 reference, have been reported.[99,100] A donor-acceptor conjugated copolymer consisting of the 2,7-diethynylfluorene as electron-accepting site and *N*,*N*,*N*′,*N*′-tetrakis(4-phenyl)-4,4′-diamino-1,1′-biphenyl as electron-donating site exhibited the γ value of 450×10^{-32} esu.[100] On the other hand, a C_{60} derivative with electron donor, $-(NH_2)_2CNCN$, was estimated as 3.5×10^{-32} esu.[99] These data may be directly comparable to our porphyrin system as summarized in Table 5.

Several factors may contribute to the large enhancement of the nonlinearity. However, the huge increments of $\lvert\gamma_{yyyy}\rvert$ values by two orders of magnitude were observed when free base porphyrins are attached at the terminal positions of core zinc complexes, **38**–**40**. These data clearly showed that the combination of terminal free base and core zinc porphyrin moiety is important to enhance the nonlinearity. The terminal free base, working as a primary electron acceptor in photosynthetic reaction centers, is certainly regarded as the acceptor with respect to the inner Zn-porphyrin. Compounds **38**–**40** are therefore regarded as a class of linear quadrapolar molecules,[24] which consist of polarizable π-electronic systems at the central core and acceptors at the molecular terminal. π-Stacked complementary coordination of imidazolyl to Zn-porphyrin must be an efficient method to produce polarizable π-electronic systems. According to the methodology here presented, the molecular length and the structure of central π-conjugation system are easily modified. It is beneficial that specific terminal groups, not only of acceptor, but also of donor and donor/acceptor pair, can be introduced simply by coordination reorganization.

5. Conclusions

We have applied supramolecular techniques such as ligand to central metal coordination, hydrogen bonding, and chelate complexation to external metal ion to construct self-assembled porphyrin arrays that are useful in artificial photosynthesis and as molecular electronic/photonic materials. The complementary coordination of imidazolyl to central zinc allowed us to construct a good special pair model and to open the way to further propagated multi porphyrin arrays by directly linking two coordination units. Porphyrin assemblies can be dissociated into monomeric species by adding a competing ligand such as MeOH or pyridine; a specific molecular terminator can be simply introduced to exhibit the efficient generation of photocurrent with light-harvesting function and the large NLO response applicable to ultrafast optical switching. These trials are now under development by modification of molecular structures to obtain even more excellent photoelectric conversion and optical functions as well as single molecular devices.

Many efforts to understand the mechanism of natural photosynthetic process have been made by construction of covalently or non-covalently linked multi-porphyrin arrays.[34] We have also revealed that the simple supramolecular porphyrin arrays assisted by Ga-oxinato chelate complexation and hydrogen bonds gave light-harvesting and efficient energy transfer functions. Such light-harvesting antenna functions may be applied to efficient photocurrent generation combined with well-designed charge separation systems. There are many problems in the present world, especially in global environmental and energy resources. In order to improve these, it is important to develop a more efficient light-energy conversion system with low cost organic materials other than existing inorganic semiconductors.

The authors acknowledge Professor K. Yoshihara and Dr. I. V. Rubtsov for the fluorescence anisotropy measurements, and also Dr. T. Zhang for OKE measurements at Japan Advanced Institute of Science and Technology. We thank all group members of our laboratory at Nara Institute of Science and Technology and Shizuoka University for their efforts in contributing to this study.

References

1 G. McDermott, S. M. Prince, A. A. Freer, A. M. Hawthornthwaite-Lawless, M. Z. Papiz, R. J. Cogdell, and N. W. Isaacs, *Nature*, **374**, 517 (1995).

2 J. Koepke, X. Hu, C. Muenke, K. Schulten, and H. Michel, *Structure*, **4**, 581 (1996).

3 K. McLuskey, S. M. Prince, R. J. Cogdell, and N. W. Isaacs, *Biochemistry*, **40**, 8783 (2001).

4 J. Deisenhofer, O. Epp, K. Miki, R. Huber, and H. Michel, *J.*

Mol. Biol., **180**, 385 (1984).
5 J. P. Allen, G. Feher, T. O. Yeates, D. C. Rees, J. Deisenhofer, H. Michel, and R. Huber, *Proc. Natl. Acad. Sci. U.S.A.*, **83**, 8589 (1986).
6 J. P. Allen, G. Feher, T. O. Yeates, H. Komiya, and D. C. Rees, *Proc. Natl. Acad. Sci. U.S.A.*, **84**, 5730 (1987).
7 J. Deisenhofer, O. Epp, I. Sinning, and H. Michel, *J. Mol. Biol.*, **246**, 429 (1995).
8 A. Zouni, H.-T. Witt, J. Kern, P. Fromme, N. Krauss, W. Saenger, and P. Orth, *Nature*, **409**, 739 (2001).
9 P. Jordan, P. Fromme, H. T. Witt, O. Kukas, W. Saenger, and N. Krauss, *Nature*, **411**, 909 (2001).
10 X. Hu, T. Ritz, A. Damjanovic, and K. Schulten, *J. Phys. Chem. B*, **101**, 3854 (1997).
11 A. Aviram and M. A. Ratner, *Chem. Phys. Lett.*, **29**, 277 (1974).
12 "Molecular Electronics-Science and Technology," ed by A. Aviram and M. A. Ratner, Annals of the New York Academy of Sciences (1998).
13 "Molecular Electronic Devices II," ed by F. L. Carter, Marcel Dekker, New York (1987).
14 R. W. Keyes, *Physics Today*, **45**, 42 (1992).
15 Y. Wada, "Molecular Electronics-Science and Technology," ed by A. Aviram and M. A. Ratner, Annals of the New York Academy of Sciences, **852**, 257 (1998).
16 H. Dai, J. Kong, C. Zhou, N. Franklin, T. Tombler, A. Cassell, S. Fan, and M. Chapline, *J. Phys. Chem. B*, **103**, 11246 (1999).
17 Z. Yao, H. W. Ch. Postma, L. Balents, and C. Dekker, *Nature*, **402**, 273 (1999).
18 J.-H. Chou, M. E. Kosal, H. S. Nalwa, N. A. Rakow, and K. S. Suslick, "The Porphyrin Handbook," ed by K. Kadish, K. M. Smith, and R. Guilard, Academic Press, New York (1999), Vol. 6, p. 43.
19 "Introduction to Nonlinear Optical Effects in Molecules and Polymers," ed by P. N. Prasad and D. J. Williams, Wiley, New York (1991).
20 "Molecular Nonlinear Optics: Materials, Physics and Devices," ed by J. Zyss, Academic Press, Boston (1994).
21 C. Bosshard, K. Sutter, P. Prêtre, J. Hulliger, M. Flörsheimer, P. Kaatz, and P. Günter, "Organic Nonlinear Optical Materials," Gordon and Breach, Amsterdam (1995).
22 G. Chen and S. Mukamel, *J. Phys. Chem.*, **100**, 11080 (1996).
23 R. R. Tykwinski, U. Gubler, R. E. Martin, F. Diederich, C. Bosshard, and P. Günter, *J. Phys. Chem. B*, **102**, 4451 (1998).
24 S. Hahn, D. Kim, and M. Cho, *J. Phys. Chem. B*, **103**, 8221 (1999), and references therein.
25 C. Maloney, H. Byrne, W. M. Dennis, W. Blau, and J. M. Kelly, *Chem. Phys.*, **121**, 21 (1988).
26 T. Sakaguchi, Y. Shimizu, M. Miya, T. Fukumi, K. Ohta, and A. Nagata, *Chem. Lett.*, **1992**, 281.
27 S. Guha, K. Kang, P. Porter, J. F. Roach, D. E. Remy, F. J. Aranda, and D. V. G. L. N. Rao, *Opt. Lett.*, **17**, 264 (1992).
28 F. Z. Henari, W. J. Blau, L. R. Milgrom, G. Yahioglu, D. Phillips, and J. A. Lacey, *Chem. Phys. Lett.*, **267**, 229 (1997).
29 M. Terazima, H. Shimizu, and A. Osuka, *J. Appl. Phys.*, **81**, 2946 (1997).
30 J. R. G. Thorne, S. M. Kuebler, R. G. Denning, I. M. Blake, P. N. Taylor, and H. L. Anderson, *Chem. Phys.*, **248**, 181 (1999).
31 S. M. Kuebler, R. G. Denning, and H. L. Anderson, *J. Am. Chem. Soc.*, **122**, 339 (2000).
32 T. E. O. Screen, J. R. G. Thorne, R. G. Denning, D. G. Bucknall, and H. L. Anderson, *J. Am. Chem. Soc.*, **124**, 9712 (2002).
33 K. Ogawa, T. Zhang, K. Yoshihara, and Y. Kobuke, *J. Am. Chem. Soc.*, **124**, 22 (2002).
34 D. Gust and T. A. Moore, "The Porphyrin Handbook," ed by K. Kadish, K. M. Smith, and R. Guilard, Academic Press, New York (1999), Vol. 8, p. 154.
35 H. L. Anderson, *Chem. Commun. (Cambridge, U.K.)*, **1999**, 2323.
36 A. A. Bothner-By, J. Dadok, T. E. Johnson, and J. S. Lindsey, *J. Phys. Chem.*, **100**, 17551 (1996).
37 N. Aratani and A. Osuka, *Bull. Chem. Soc. Jpn.*, **74**, 1361 (2001).
38 A. Tsuda and A. Osuka, *Science*, **293**, 79 (2001).
39 V. S.-Y. Lin, S. G. Dimagno, and M. J. Therien, *Science*, **264**, 1105 (1994).
40 U. Michelsen and C. A. Hunter, *Angew. Chem. Int. Ed.*, **39**, 1458 (2000).
41 K. Ogawa and Y. Kobuke, *Angew. Chem. Int. Ed.*, **39**, 4070 (2000).
42 A. Ambroise, R. W. Wagner, P. D. Rao, J. A. Riggs, P. Hascoat, J. R. Diers, J. Seth, R. K. Lammi, D. F. Bocian, D. Holten, and J. S. Lindsey, *Chem. Mater.*, **13**, 1023 (2001).
43 D. Holten, D. F. Bocian, and J. S. Lindsey, *Acc. Chem. Res.*, **35**, 57 (2002).
44 K. Sugiura, H. Tanaka, T. Matsumoto, T. Kawai, and Y. Sakata, *Chem. Lett.*, **1999**, 1193.
45 C. C. Mac, D. Pomeranc, M. Montalti, L. Prodi, and J. K. M. Sanders, *Chem. Commun.*, **1999**, 1083.
46 L. Ruhlmann, A. Schulz, A. Giraudeau, C. Messerschmidt, and J.-H. Fuhrhop, *J. Am. Chem. Soc.*, **121**, 6664 (1999).
47 K. Funatsu, T. Imamura, A. Ichimura, and Y. Sasaki, *Inorg. Chem.*, **37**, 4986 (1998).
48 Y. Kobuke and H. Miyaji, *J. Am. Chem. Soc.*, **116**, 4111 (1994).
49 Y. Kobuke and H. Miyaji, *Bull. Chem. Soc. Jpn.*, **69**, 3563 (1996).
50 H. Miyaji and Y. Kobuke, *Mol. Cryst. Liq. Cryst.*, **276**, 283 (1996).
51 Y. Kobuke and N. Nagata, *Mol. Cryst. Liq. Cryst.*, **342**, 51 (2000).
52 A. Nomoto and Y. Kobuke, *Chem Commun. (Cambridge, U.K.)*, **2002**, 1104.
53 I. V. Rubtsov, Y. Kobuke, H. Miyaji, and K. Yoshihara, *Chem. Phys. Lett.*, **308**, 323 (1999).
54 Y. Kobuke, H. Miyaji, and K. Ogawa, *Suplamol. Chem.*, **14**, 159 (2002).
55 Y. Tomohiro, A. Satake, and Y. Kobuke, *J. Org. Chem.*, **66**, 8442 (2001).
56 N. Nagata, S. Kugimiya, and Y. Kobuke, *Chem. Commun. (Cambridge, U.K.)*, **2000**, 1389.
57 N. Nagata, S. Kugimiya, and Y. Kobuke, *Chem. Commun. (Cambridge, U.K.)*, **2001**, 689.
58 C. K. Chang and I. Abdalmuhdi, *Angew. Chem., Int. Ed. Engl.*, **23**, 164 (1984).
59 A. Osuka and K. Murayama, *J. Am. Chem. Soc.*, **110**, 4454 (1988).
60 A. Osuka, S. Nakajima, T. Nagata, K. Murayama, and K. Toriumi, *Angew. Chem., Int. Ed. Engl.*, **30**, 582 (1991).
61 H. Meier, Y. Kobuke, and S. Kugimiya, *J. Chem. Soc., Chem. Commun.*, **1989**, 923.
62 C. M. Drain, R. Fischer, E. G. Nolen, and J.-M. Lehn, *J. Chem. Soc., Chem. Commun.*, **1993**, 243.

63 Y. Kuroda, A. Kawashima, T. Urai, and H. Ogoshi, *Tetrahedon Lett.*, **36**, 8449 (1995).
64 Y. Kuroda, A. Kawashima, Y. Hayashi, and H. Ogoshi, *J. Am. Chem. Soc.*, **119**, 4929 (1997).
65 R. T. Stibrany, J. Vasudevan, S. Knapp, J. A. Potenza, T. Emge, and H. J. Schugar, *J. Am. Chem. Soc.*, **118**, 3980 (1996).
66 C. A. Hunter and L. D. Sarson, *Angew. Chem., Int. Ed. Engl.*, **33**, 2313 (1994).
67 Y. Inaba, A. Nomoto, and Y. Kobuke, unpublished work. X-ray crystallographic data will be published elsewhere.
68 H. Miyaji, Y. Kobuke, and J. Kondo, *Chem. Lett.*, **1996**, 497.
69 M. Kasha, H. R. Rawls, and M. A. El-bayyoumi, *Pure Appl. Chem.*, **11**, 371 (1965).
70 J. H. Fendler, ''Membrane Mimetic Chemistry,'' John Wiley and Sons, Inc. (1982).
71 H. L. Tavernier, A. V. Barzykin, M. Tachiya, and M. D. Fayer, *J. Phys. Chem. B*, **102**, 6078 (1998).
72 M. Merritt, M. Lanier, G. Deng, and S. L. Regen, *J. Am. Chem. Soc.*, **120**, 8494 (1998).
73 T. Komatsu, E. Tsuchida, C. Böttcher, D. Donner, C. Messerschmidt, U. Siggel, W. Stocker, J. P. Rabe, and J.-H. Fuhrhop, *J. Am. Chem. Soc.*, **119**, 11660 (1997).
74 H. Komatsu and P. L.-G. Chong, *Biochemistry*, **37**, 107 (1998).
75 R. Ballardini,G. Varani, M. T. Indelli, and F. Scandola, *Inorg. Chem.*, **25**, 3858 (1986).
76 H. Schmidbaur, J. Lettenbauer, D. L. Wilkinson, G. Müller, and O. Kumberger, *Z. Naturforsch., B: Chem. Sci.*, **46**, 901 (1991).
77 C. W. Tang and S. A. VanSlyke, *Appl. Phys. Lett.*, **51**, 913 (1987).
78 C. W. Tang, S. A. VanSlyke, and C. H. Chen, *J. Appl. Phys.*, **65**, 3610 (1989).
79 M. Linke, J.-C. Chambron, V. Heitz, J.-P. Sauvage, and V. Semetey, *Chem. Commun. (Cambridge, U.K.)*, **1998**, 2469.
80 A. P. de Silva, H. Q. N. Gunaratne, T. Gunnlaugsson, A. J. M. Huxley, C. P. McCoy, J. T. Rademacher, and T. E. Rice, *Chem. Rev.*, **97**, 1515 (1997).
81 J.-P. Collin, C. Dietrich-Buchecker, P. Gaviña, M. C. Jimenez-Molero, and J.-P. Sauvage, *Acc. Chem. Res.*, **34**, 477 (2001).
82 J.-P. Sauvage, *Acc. Chem. Res.*, **31**, 611 (1998).
83 V. Balzani, A. Credi, F. M. Raymo, and J. F. Stoddart, *Angew. Chem. Int. Ed.*, **38**, 3348 (2000).
84 M. F. Semmelhack, P. Helquist, L. D. Jones, L. Keller, L. Mendelson, L. S. Ryono, J. G. Smith, and R. D. Stauffer, *J. Am. Chem. Soc.*, **103**, 6460 (1981).
85 T. Yamamoto, Z. Zhou, T. Kanbara, and T. Maruyama, *Chem. Lett.*, **1990**, 223.
86 M. Iyoda, H. Otsuka, K. Sato, and M. Oda, *Bull. Chem. Soc. Jpn.*, **63**, 80 (1990).
87 A. Osuka and H. Shimidzu, *Angew. Chem., Int. Ed. Engl.*, **36**, 135 (1997).
88 A. Nakano, A. Osuka, I. Yamazaki, T. Yamazaki, and Y. Nishimura, *Angew. Chem. Int. Ed.*, **37**, 3023 (1998).
89 T. Ogawa, Y. Nishimoto, N. Yoshida, N. Ono, and A. Osuka, *Angew. Chem. Int. Ed.*, **38**, 176 (1999).
90 N. Yoshida and A. Osuka, *Org. Lett.*, **2**, 2963 (2000).
91 K. Uosaki, T. Kondo, X.-Q. Zhang, and M. Yanagida, *J. Am. Chem. Soc.*, **119**, 8367 (1997).
92 H. Imahori and Y. Sakata, *Eur. J. Org. Chem.*, **1999**, 2445.
93 H. Imahori, H. Yamada, Y. Nishimura, I. Yamazaki, and Y. Sakata, *J. Phys. Chem. B*, **104**, 2099 (2000).
94 H. Imahori, H. Norieda, H. Yamada, Y. Nishimura, I. Yamazaki, Y. Sakata, and S. Fukuzumi, *J. Am. Chem. Soc.*, **123**, 100 (2001).
95 H. Imahori, M. Arimura, T. Hanada, Y. Nishimura, I. Yamazaki, Y. Sakata, and S. Fukuzumi, *J. Am. Chem. Soc.*, **123**, 335 (2001).
96 A. Aoki, Y. Abe, and T. Miyashita, *Langmuir*, **15**, 1463 (1999).
97 H. Imahori, H. Norieda, S. Ozawa, K. Ushida, H. Yamada, T. Azuma, K. Tamaki, and Y. Sakata, *Langmuir*, **14**, 5335 (1998).
98 H. Imahori, H. Norieda, Y. Nishimura, I. Yamazaki, K. Higuchi, N. Kato, T. Motohiro, H. Yamada, K. Tamaki, M. Arimura, and Y. Sakata, *J. Phys. Chem. B*, **104**, 1253 (2002).
99 S. Wang, W. Huang, R. Liang, and Q. Gong, *Phys. Rev. B*, **63**, 153408 (2001).
100 X. Zhan, Y. Liu, D. Zhu, W. Huang, and Q. Gong, *Chem. Mater.*, **13**, 1540 (2001).

Yoshiaki Kobuke was born in Amagasaki, Hyogo in 1941. He received his Ph. D. degree from Kyoto University in 1970. This year he started an academic career at the Department of Synthetic Chemistry, Kyoto University as an assistant professor. In 1972-1973, he spent a year at the Department of Chemistry, Harvard University. After promotion to an associate professor at Kyoto University, he moved in 1990 to the Department of Materials Science, Shizuoka University as a professor. In 1998, he moved to the Graduate School of Materials Science, Nara Institute of Science and Technology. Since 1998, he has been a project leader of CREST, JST for the research theme "Total Construction of Energy Conversion and Signal Transduction Systems in Biology". His research interest covers supramolecular approaches toward biological functions, such as photosynthesis and signal transduction systems.

Kazuya Ogawa was born in Kitami, Hokkaido, Japan, in 1970. He received his Ph. D. degree in 1999 from Hokkaido University. He has been a postdoctoral researcher of CREST, JST on the development of self-assmbled porphyrin arrays since 1999 and an assistant professor since 2001 at the Graduate School of Materials Science, Nara Institute of Science and Technology. His current research has focused on the development of molecular photonic/electronic materials and artifical photosynthesis by self-assmbled porphyrin systems.